Target-specific requirements for RNA interference can be explained by a single regulatory network

Daphne R. Knudsen[1], Pravrutha Raman[1,2], Farida Ettefa[1,3], Laura De Ravin[1], and Antony M. Jose[1]

[1]Department of Cell Biology and Molecular Genetics, University of Maryland, College Park, USA. Biological Sciences Graduate Program, University of Maryland, College Park, USA.

[2]Current address: Division of Basic Sciences, Fred Hutchinson Cancer Research Center, Seattle, WA, USA.

[3]Current address: Institute for Systems Genetics, New York University School of Medicine, New York, NY, USA.

*Corresponding author: Antony M. Jose

Email: amjose@umd.edu

Author Contributions: All authors contributed to experimental design and analysis. D.R.K., P.R., F.E., and L.D.R. performed experiments; A.M.J. wrote scripts for quantitative modeling that were confirmed and adapted to R by D.R.K.; D.R.K. and A.M.J. wrote the manuscript.

Competing Interest Statement: The authors declare no conflict of interest.

Classification: Biological sciences; Genetics

Keywords: RNA interference, epigenetics, regulation of gene expression

This PDF file includes:

Main Text

Figs.1 to 5

Figs.S1 to S4

Tables S1 to S3

Abstract

Since double-stranded RNA (dsRNA) is effective for silencing a wide variety of genes, all genes are typically considered equivalent targets for such RNA interference (RNAi). Yet, loss of some regulators of RNAi in the nematode *C. elegans* can selectively impair the silencing of some genes, raising the possibility of gene-specific specialization of the RNAi mechanism. Here we dissect the silencing of two somatic genes in detail to show that such selective regulation can be explained by a single network of regulators acting on genes with differences in their RNA metabolism. In this network, the Maelstrom domain-containing protein RDE-10, the intrinsically disordered protein MUT-16, and the Argonaute protein NRDE-3 work together so that any two are required for silencing one gene, but each is singly required for silencing the other gene. While numerous features could distinguish one gene from another, quantitative models suggest that, for the same steady state abundance of mRNA, genes with higher rates of mRNA production are more difficult to knockdown with a single dose of dsRNA and recovery from knockdown can occur if all intermediates of RNA silencing turnover. Consistent with such dissipation of RNA silencing, animals recover after silencing by a pulse of dsRNA and show restricted production of templates for amplifying small RNAs. The loss of NRDE-3 can be overcome by enhancing dsRNA processing, which supports a quantitative contribution of this regulator to RNA silencing. These insights explain selectivity in the requirements for specific regulators without invoking different mechanisms for different sets of genes.

Significance Statement

RNA interference (RNAi) is a widely used mechanism for silencing the expression of genes to combat disease or improve agriculture. We show that different genes can show stark differences in their requirements for particular regulators of RNAi despite silencing relying on a single regulatory network. These differences are explained by genes having different thresholds for silencing such that genes with high thresholds for silencing require multiple regulators of RNA silencing for efficient knockdown. When such genes are targeted, resistance through mutations becomes more likely, necessitating another round of drug development. Anticipating these mechanisms for the development of resistance before widespread use of an RNAi-based drug or treatment will be crucial for avoiding futile cycles of innovation.

Main Text

Introduction

Double-stranded RNA (dsRNA) can trigger the conserved mechanism of RNA interference (RNAi) to degrade mRNA of matching sequence (1), and thus silence gene expression, in many organisms. This conservation has made dsRNA-based drugs useful in crops (2), insects (3), and humans (4). While a dsRNA-based drug can be designed using just the mRNA sequence of any target gene, the intracellular effectiveness of the drug and the ease with which an organism could escape the drug by developing resistance are difficult to predict. Predicting both efficacy and susceptibility to resistance for each target could inform the selection of a suitable target from two or more equivalent candidates. Extensive characterization of RNAi in the nematode *C. elegans* (reviewed in ref. (5)) makes it a suitable system to examine how differences between target genes and reliance on specific regulators contribute to efficacy and resistance.

A skeletal pathway that is required for gene silencing in response to the addition of dsRNA has been worked out in *C. elegans* (Fig. 1A). Long dsRNA is imported through the transmembrane protein SID-1 (6,7), after which it is bound by the dsRNA-binding protein RDE-4 (8), which recruits the endonuclease DCR-1 (9) to cleave the long dsRNA into smaller dsRNAs (10). The primary Argonaute protein RDE-1 (11, 12) cleaves one strand of the dsRNA (13) and associates with the other, making it a 1º short interfering RNA (siRNA) that can guide the recognition of target mRNAs of matching sequence (siRNAs; processing, pink). After recognition by RDE-1-bound siRNAs, the target mRNAs are cleaved and the 5' fragments are stabilized through the addition of 3' UG-dinucleotide repeats (14) by the nucleotidyltransferase RDE-3 (15) to form pUG RNAs (16), which act as templates for the amplification of 2º siRNAs (17) by RNA-dependent RNA polymerases. This amplification of silencing signals through the production of 2º siRNAs is facilitated by the intrinsically disordered protein MUT-16 (19, 20), the Maelstrom domain-containing protein RDE-10 (21, 22), and their interactors (20-23). These 2º siRNAs are bound by one of several Argonautes (24), resulting in the eventual degradation of target mRNAs in the cytoplasm, which requires a cytoplasmic Argonaute, and/or co-transcriptional silencing of the target gene in the nucleus, which requires a nuclear Argonaute (e.g., NRDE-3 (25) in somatic cells). Although it is difficult to compare the silencing of two different genes by controlling all relevant variables, past studies have highlighted gene-specific differences

in the efficacy of RNAi under different conditions (e.g., when RNAi is enhanced through the loss of the exonuclease ERI-1 (26), when nuclear silencing is blocked in somatic cells through loss of NRDE-3 (27), or when different concentrations of dsRNA are used (28)). Understanding the sources of such differences and the underlying mechanisms will improve our ability to design efficacious dsRNA drugs that are difficult to evade through the development of resistance.

Here we analyze the requirements for silencing two exemplar genes and use quantitative modeling to advance a parsimonious view of RNAi in somatic cells. We show that MUT-16, RDE-10, and NRDE-3 each is required for the silencing of *bli-1,* but any two of these proteins are sufficient for *unc-22* silencing. These differences can be explained by differences in the thresholds for silencing the two genes using a single network of regulators. A dynamic model of RNA changes during silencing by dsRNA reveals several criteria for efficient RNA silencing and suggests that targets can recover expression over time despite the presence of mechanisms that amplify silencing signals. These insights from modeling are supported by experimental results demonstrating the recovery of animals after a pulse of RNAi, a dearth of pUG RNA production by 2º siRNAs, and the bypass of some genetic requirements when the processing of dsRNA is enhanced.

Results

Two genes with different thresholds for silencing reveal a web of regulators that mediate RNA interference

To identify regulators of RNA interference (RNAi), we performed a primary screen for mutants that disrupt silencing in the germline in response to mating (29) followed by a secondary screen for silencing of two somatic genes in response to ingestion of bacteria expressing dsRNA of matching sequence (30). We mutagenized a strain with stable RNA silencing in the germline initiated by mating (29) and isolated 15 viable mutants that showed re-expression (Fig. S1A). Using whole-genome sequencing followed by in silico complementation (see Methods), we identified five mutants that had premature stop codons in *mut-16* (Fig. 1B), a known regulator of RNAi that is required for the production of secondary siRNAs (19, 20, 23). MUT-16 is required for the silencing of all tested somatic targets except the muscle gene *unc-22* (19), which is considered a sensitive target for RNAi (1). While all five putative *mut-16* mutants failed to silence the

hypodermal gene *bli-1* (Fig. 1C, *left*), only one of the five failed to silence the muscle gene *unc-22* (Fig. 1C, *right*). Upon further analysis of the mutant that failed to silence *unc-22*, we found that this mutant also contained a missense mutation in RDE-10, another known regulator of RNAi that is required for the production of secondary siRNAs (21, 22). This missense mutation (Ser228Phe) is expected to disrupt the Maelstrom domain of RDE-10 (Fig. S1C), and thus could result in a loss of RDE-10 function. To eliminate possible confounding effects of multiple mutations in strains isolated from a genetic screen, we used Cas9-mediated genome editing to introduce mutations in *mut-16* (null) and/or *rde-10* (null or a missense mutation that encodes Ser228Phe) in a wild-type background (Fig. 1B). While the newly created *mut-16(null)* mutants showed *unc-22* silencing as expected, *mut-16(null) rde-10(null)* (Fig. 1D, *right*) double mutants failed to silence *unc-22*. These observations suggest that MUT-16 and RDE-10 are redundantly required for silencing *unc-22* and that the Maelstrom domain of RDE-10 is required for this function. Since the primary Argonaute RDE-1 is required for the silencing of all somatic targets (Fig. 1A; (11,12)), including *unc-22*, we propose that MUT-16 and RDE-10 act in parallel downstream of RDE-1 to promote the amplification of 2º siRNA.

Two observations suggest differences in the requirements for silencing *bli-1* and *unc-22*. One, like *mut-16(-)* single mutants, *rde-10(-)* single mutants failed to silence *bli-1* but not *unc-22* (Fig. 1D). Two, animals that lack the nuclear Argonaute NRDE-3 fail to silence *bli-1* but can silence *unc-22* (27). Since *rde-10(-); nrde-3(-)* double mutants fail to silence *unc-22* (21), one unifying explanation is that NRDE-3 functions downstream of MUT-16 in parallel to RDE-10. To test this possibility, we generated *nrde-3(-)* mutants using genome editing (Fig. 2A) and compared silencing in single mutant and double mutant combinations using the newly generated mutants lacking *mut-16*, *rde-10*, or *nrde-3*. As expected, all single mutants failed to silence *bli-1* but silenced *unc-22*. Surprisingly, all double mutants failed to silence both *bli-1* and *unc-22* (Fig. 1D and 2B). This requirement for any two of MUT-16, RDE-10, and NRDE-3 suggests that the RNAi pathway must branch downstream of both MUT-16 and RDE-10 - each protein cannot be upstream of the other two.

The stark differences in the extents of silencing *bli-1* (~0%) versus *unc-22* (~100%) (Fig. 1D and 2B) in animals lacking *mut-16*, *rde-10*, or *nrde-3* suggest that there could be target-specific pathways for silencing, or more parsimoniously, that MUT-16, RDE-10, and NRDE-3 each contribute to the silencing of

both targets as part of a single network (Fig. 2C) with *unc-22* being more sensitive to silencing than *bli-1*. For such a single network with quantitative contributions by multiple regulators of RNAi to explain the silencing of somatic targets, including targets like *unc-22* and *bli-1* that show dramatic differences, it should be possible to identify values for the relative contributions of each regulatory path ($\mathcal{N}m$ = from MUT-16 to NRDE-3, $\mathcal{N}r$ = from RDE-10 to NRDE-3, $\mathcal{O}m$ = from MUT-16 to other Argonautes, and $\mathcal{O}r$ = from RDE-10 to other Argonautes in Fig. 2C, *left*) and for gene-specific thresholds ($T_{bli\text{-}1}$ = level of BLI-1 function below which a defect is detectable, and $T_{unc\text{-}22}$ = level of UNC-22 function below which a defect is detectable) that are consistent with all experimental data ('constraints' in Fig. 2C, *right*). Of the 100,000 sets of parameters simulated, 145 sets satisfied all experimental constraints (Fig. 2D). These allowed parameter sets were obtained despite the conservative assumption that the levels of mRNA knockdown for detecting observable defects for *bli-1* and *unc-22* are similar. Relaxing this assumption will lead to a larger number of allowed parameter sets. These valid parameter sets included cases with different relative contributions from RDE-10 and MUT-16 to NRDE-3-dependent silencing for a range of threshold differences for silencing *bli-1* versus *unc-22* (Fig. 2D, left). Furthermore, extreme contributions of MUT-16 versus RDE-10 (Fig. 2D, middle) or NRDE-3 versus other Argonautes (Fig. 2D, right) were excluded. Finally, only thresholds for *bli-1* silencing that are less than ~5.5x the threshold for *unc-22* silencing were supported despite the allowed range of up to 100x (Fig. 2D). Taken together, our data are consistent with a single network for RNAi targeting somatic genes where multiple regulatory pathways provide quantitative contributions to silencing.

Quantitative modeling of RNA interference and mRNA production predicts a variety of target-specific outcomes

The many protein regulators of RNAi drive changes in RNA metabolism, including the production of new RNA species (1º siRNA, 2º siRNA, and pUG RNA), that are associated with the targeted gene. Although these changes can be indicators of RNA silencing, the quantitative relationship between such RNA intermediates and the extent of gene silencing measured as a reduction in function of the targeted gene or its mRNA levels is unclear. A priori, reduction in the mRNA levels of a gene could depend on universal processing of imported dsRNA, production of secondary small RNAs with the participation of gene-specific mRNAs, and downregulation of pre-mRNA and mRNA influenced by pre-existing gene-specific RNA

metabolism. To understand how these gene-specific factors could influence RNA silencing, we began by analyzing the impact of a few characteristics of a gene on mRNA and pre-mRNA levels after RNAi using a sequential equilibrium model (Fig. S2A and Supplemental Methods). Exploration of the parameter sets that supported knockdown with residual presence of target RNAs (790 of 1 million simulated with $[m]_i < [m]$, $[m]_i > 0$, and $[p]_i > 0$; Fig. S2B) revealed that (1) RNAi can result in different residual concentrations of RNAs for different genes (Fig. S2C); (2) for a given gene, silencing can alter the ratio of pre-mRNA to mRNA (Fig. S2D and S2E); and (3) effective targeting of mRNA by primary or secondary small RNAs is required for strong silencing (Fig. S2F). These analyses hint at the influence of gene-specific factors on the functional outcome of RNAi and impel the exploration of a detailed dynamic model.

Early quantitative models of RNAi (e.g., ref. (31)) were proposed before crucial discoveries on the biogenesis of 2º siRNAs without forming long dsRNA (17) and the stabilization of mRNA templates as pUG RNAs (14, 16). Therefore, we incorporated these developments and modeled how the addition of dsRNA could disrupt the steady-state RNA metabolism of the targeted gene using ordinary differential equations (Fig. 3A). The steady-state levels of pre-mRNA and mRNA - which depend on production, maturation, and turnover - could be altered upon the addition of matching dsRNA through the generation of new RNA species (1º siRNA, 2º siRNA, pUG RNA) that are also subject to turnover. To accommodate these known intermediates and interactions, we used six differential equations to describe the rate of change of key RNA species (dsRNA (*ds*), 1º siRNA (*pri*), pUG RNA (*ug*), 2º siRNA (*sec*), pre-mRNA (*p*), and mRNA (*m*)) with rate or binding constants for different processes (*k1* through *k9*), turnover rates for different RNAs (T_{pri}, T_{ug}, T_{sec}, T_p, T_m), and variables for the lengths of RNAs (l_{ds} - dsRNA; l_m - mRNA).

To illustrate the relative dynamics of different RNA species upon the addition of dsRNA, we computed the concentrations of dsRNA, 1º siRNA, pUG RNA, 2º siRNA, pre-mRNA, and mRNA using the equations after assigning arbitrary values for the different constants (Fig. 3B; see legend for parameter values). As expected, the levels of dsRNA decay (Fig. 3B, red) as it is processed into 1º siRNA (Fig. 3B, purple), which eventually decays because of turnover. This transient accumulation of 1º siRNA is followed by that of pUG RNAs (Fig. 3B, green) and of 2º siRNA (Fig. 3B, brown). Silencing of the target is reflected in the lowered levels of mRNA (Fig. 3B, blue) and pre-mRNA (Fig. 3B, orange). However, these levels eventually recover upon turnover of the silencing intermediates (1º siRNA, pUG RNA, 2º siRNA). For any

gene, the time to knockdown (τ_{kd}) and the duration of knockdown (t_{kd}) could be used to evaluate the efficiency of RNAi (knockdown = 10% of initial mRNA concentration in Fig. 3B). The many RNA species made downstream of 1º RNA binding in *C. elegans* provide the opportunity for multiple parameters to differ between genes. Therefore, we varied each parameter and examined τ_{kd} and t_{kd} as indicators of efficiency (Fig. S3). Overall, τ_{kd} and t_{kd} were uncorrelated (Fig. 3C), with cases of rapid but transient knockdown, which would necessitate multiple dosing of dsRNA for sustained effects. While loss of function or reduction of mRNA levels are often the intended goals of knockdown, RNA intermediates could serve as convenient and quantitative measures of molecular changes. For example, the abundant 2º siRNAs have been a widely used molecular indicator of silencing (e.g., ref. (32)). However, the maximal amount of 2º siRNAs that accumulate is not correlated with strong silencing as measured by the minimal amount of mRNA during knockdown (Fig. 3D). Additionally, an increase in transcription generally resulted in poorer knockdown through changes in both τ_{kd} and t_{kd} (Fig. 3E), suggesting that a gene with transcriptional upregulation during exposure to dsRNA will be more difficult to knockdown.

Efficient silencing using dsRNA is possible in many organisms, including mammals, despite silencing relying on mostly post-transcriptional degradation of mRNA without the production of pUG RNA or 2º siRNA (33). To explore differences between genes that could impact the efficiency of RNA silencing universally in any system, we simulated knockdown through the post-transcriptional loss of mRNA alone by eliminating production of pUG RNAs, and thus downstream secondary small RNAs and transcriptional silencing (Fig. 3A, *k3* = 0). We found that when a fixed amount of dsRNA was exposed to different genes with the same amount of mRNA at steady state, genes with higher mRNA turnover rates showed less efficient knockdown (Fig. 3F). This inverse relationship is expected because to maintain the same steady state levels, genes with higher mRNA turnover must also have higher mRNA production.

In summary, varying a few gene-specific parameters revealed the diversity of outcomes that are possible in response to the same dose of dsRNA. Gene-specific differences make the time to knockdown and the duration of knockdown uncorrelated and reduce the utility of key intermediates of RNA silencing as

predictors of knockdown efficiency. Increases in transcription during exposure to dsRNA and high turnover of mRNA coupled with high production at steady state reduce the efficiency of knockdown.

Gene expression can recover after knockdown despite the presence of amplification mechanisms

A key prediction of the quantitative model is that animals can recover from RNA silencing because of the turnover of silencing signals despite the production of abundant 2º siRNAs using RNA-dependent RNA polymerases. Experimental detection of the re-establishment of wild-type phenotype after a pulse of RNAi would provide evidence not only for the recovery of mRNA levels but also the subsequent production of functional protein. To test this possibility, we exposed animals to a 1-hr pulse of dsRNA targeting the sensitive target *unc-22* and examined them for the Unc-22 defect every 24 hours (Fig. 4A). With this limited exposure to dsRNA, we observed only ~80% silencing after the first 24 hours, which reached ~100% by day 3, suggesting that it takes a couple of days after exposure to small amounts of dsRNA to observe complete silencing. This delay could be driven by the time required for the buildup of RNA intermediates required for silencing (1º siRNA, 2º siRNA, and/or pUG RNA), for the turnover of UNC-22 protein, and/or for the dissipation of events downstream of the molecular role of UNC-22. Consistent with recovery, silencing was only observed in ~50% of the animals on day 5, which dropped to ~36% by the eighth day after RNAi. In contrast, animals that were continually fed *unc-22* RNAi showed ~100% silencing even at day 7 (Fig. 4A), suggesting that the RNAi machinery remains functional in aging animals. Thus, these results support the turnover of all key RNA intermediates generated during RNAi – 1º siRNA, 2º siRNA, and pUG RNA.

Of these intermediates, pUG RNAs have been proposed to be stable templates for the production of small RNAs (16). Sustained production of small RNAs could occur if the targeting of mRNA by 2º siRNA resulted in further pUG RNA production, subsequent 3º siRNA production, and so on, thereby providing a way for silencing to persist despite the turnover of all RNA species. However, the production of such 3º siRNA was only observed when targeting a germline gene (34) and not when targeting a somatic gene (18). To examine whether such repeated rounds of pUG RNA production occur during RNAi of *unc-22*, we fed wild-type worms bacteria that express *unc-22* dsRNA or control dsRNA (L4440) and looked for the presence of pUG RNAs. These RNAs are detected as a heterogenous mixture using RT-PCR with a poly-AC 3' primer

and gene-specific 5' primers. Consistent with the production of pUG RNAs upon targeting by 1º siRNAs, we detected pUG RNAs generated after cleavage within the *unc-22* mRNA sequence that matches the dsRNA (Fig. 4B, 0kb 5' primer). Since, 2º siRNAs are made with a 5' bias on the mRNA template (17, 18) pUG RNAs generated in response to targeting by 2º siRNAs are expected to include mRNAs cleaved upstream of the sequence matching the dsRNA. Surprisingly, all pUG RNAs detected using a 5' primer ~1kb upstream of the target sequence were larger than 1 kb (Fig. 4B, 1kb 5' primer), suggesting that there is a dearth of pUG RNA formation through cleavage within 1 kb upstream of sequences targeted by dsRNA. Notably, this absence is despite the expected relative ease of amplifying shorter sequences when compared with amplifying longer sequences using the same primers. These results argue against pUG RNA production in response to targeting by 2º siRNAs made against a somatic gene, supporting the idea that amplification is not perpetual and that mRNA levels can thus recover over time.

Genetic requirements for silencing some genes can be bypassed by enhancing dsRNA processing

The production of pUG RNAs and 2º siRNAs requires the participation of mRNA (Fig. 3A), making the contributions of some steps during RNAi gene-specific. The resultant diversity is reflected in the many different parameter sets that support silencing (Fig. S4) and suggests that genes could differ in their dependence on proteins required for steps downstream of dsRNA processing and 1º siRNA production. Such differential dependencies can be overcome by increasing the amount of available processed dsRNA and/or 1º siRNA when alternative parallel paths are available (e.g., loss of NRDE-3 or RDE-10 in Fig. 2B) but not when no alternative paths are available (e.g., loss of both MUT-16 and RDE-10 in Fig. 2B) or when the increase is insufficient. To test these predictions, we increased dsRNA processing and examined silencing in animals lacking different regulators required for the silencing of *bli-1* and/or *unc-22*.

One approach for increasing dsRNA processing is the release of factors such as the exonuclease DCR-1 from competing endogenous pathways by removing the exonuclease ERI-1 (35). We used available *eri-1* mutants (Fig. 5A, *mg366*) and mutants generated using Cas9-mediated genome editing (Fig. 5A, *jam260* to *jam264*) to test if requirements for silencing *bli-1* and *unc-22* could be bypassed. Loss of *eri-1* enabled *bli-1* silencing in animals lacking NRDE-3, but not in animals lacking RDE-10 or MUT-16 (Fig. 5B). Furthermore, loss of *eri-1* was not sufficient for the complete rescue of *unc-22* silencing in animals lacking

any two of these three regulators (Fig. 5C). An alternative approach for increasing dsRNA processing is the overexpression of the dsRNA-binding protein RDE-4, which recruits dsRNA for processing by DCR-1 (8, 10). RNAi is expected to be particularly sensitive to changes in RDE-4 levels because minimal amounts of RDE-4 can support RNAi as evidenced by silencing in *rde-4(-)* adult progeny of *rde-4(+/-)* hermaphrodites (Fig. S7E in ref. (36)) and in *rde-4(-)* animals with trace levels of ectopic expression from multicopy *rde-4(+)* transgenes (Fig. 2 in (27)). We found that even hemizygous males expressing *rde-4(+)* from a single-copy transgene driving expression in the germline and the intestine under the control of the *mex-5* promoter (36) was sufficient for rescuing both *bli-1* and *unc-22* silencing (Fig. 5D and Fig. 5A). Similar expression of *rde-1(+)*, however, was not sufficient for rescuing silencing in *rde-1(-)* animals (Fig. 5D), suggesting that small amounts of RDE-4 but not RDE-1 is sufficient for RNAi. RDE-4 can be selectively overexpressed in the hypodermis using a single-copy transgene with a *nas-9* promoter (overexpression evident in Fig. 5E; and selectivity demonstrated in Fig. 4C in (27)). This hypodermal expression of *rde-4(+)* was sufficient to enable *bli-1* silencing in an otherwise *rde-4(-); nrde-3(-)* background (Fig. 5F). Thus, either loss of ERI-1 or overexpression of RDE-4 can bypass some of the genetic requirements for silencing *bli-1*, suggesting that the requirement for a single regulator (e.g., the Argonaute NRDE-3) does not reflect selectivity in regulation but reflects a larger amount of silencing signals required for reducing *bli-1* function sufficiently to cause a detectable defect.

Taken together, these results support the idea that gene-specific requirements for some proteins that function in RNAi do not reflect different pathways for silencing different genes, but rather a quantitative requirement for regulators acting as part of a single RNA regulatory network (Fig. 5G).

Discussion

Our results suggest that a single network of regulators can explain silencing of somatic targets of RNA interference, despite stark differences in the genetic requirements for silencing different genes. These differences can be explained by gene-specific thresholds for silencing and multiple paths to silencing downstream of dsRNA processing into primary siRNAs. A quantitative model supported by experimental results suggests the turnover of all key RNA intermediates, including pUG RNAs, which are used as templates to make numerous secondary siRNAs in *C. elegans*. Regardless of pUG RNA or secondary

siRNA production, genes with higher mRNA turnover at steady state and thus higher rates of mRNA production are more difficult to knockdown.

Universal and gene-specific requirements for RNAi. RNAi requires the entry of dsRNA into cells, the processing of dsRNA into small RNAs, recognition of target mRNA, generation of additional small RNAs, and downstream gene silencing mechanisms. The upstream processes of entry, processing, and recognition do not depend on the mRNA being targeted and are thus presumably universal. Consistently, the dsRNA importer SID-1, the endonuclease DCR-1, and the primary Argonaute RDE-1 are required for all RNAi. In contrast, since the mRNA is used as a template to generate the abundant secondary small RNAs in *C. elegans* (18) or additional dsRNAs in other systems (e.g., in plants ref. (37)), the silencing of different mRNAs could diverge through the selective recruitment of different collections of regulators. In support of this possibility, the two model genes we analyze in this study, *unc-22* and *bli-1*, show stark differences in the requirements of some RNAi factors for silencing (Fig. 1). While these differences could be attributed to their expression in different tissues, the ability to bypass some requirements (Fig. 5) argues against this possibility. Specifically, if the requirement for NRDE-3 for silencing *bli-1* (hypodermal gene) but not *unc-22* (muscle gene) is because of the lack of a parallel regulator in the hypodermis but not in the muscle, then enhancing dsRNA processing would be unable to bypass the NRDE-3 requirement (Fig. 5). Furthermore, the fact that any two of MUT-16, NRDE-3, and RDE-10 - three very structurally and functionally different genes - are required for *unc-22* silencing suggest that each of these proteins could be contributing to silencing of any RNAi target. Despite this potential use of a single network for silencing all somatic genes, different genes could critically depend on different regulators because of differences in their mRNA metabolism and/or subcellular localization, which were included in the consideration of threshold differences (Fig. 2). Intermediate steps that require the participation of mRNA such as the production of 2º siRNA could have complex dependencies, making RNA intermediates poor predictors of silencing efficiency (Fig. 3D). For example, the subcellular localization of mRNA could increase or decrease its interaction with RdRPs and thus influence the levels of 2º siRNAs made. Future studies that address the dynamics and subcellular localization of target mRNA before RNAi and the subcellular localization of components of the RNAi machinery are required to test these hypotheses.

How are 2º siRNAs made? Multiple small RNA species of defined lengths and 5'-nt bias have been detected in *C. elegans*. Of these, 22G RNAs (2º siRNAs) are the most abundant and arise from amplification downstream of exposure to dsRNA and in multiple endogenous small RNA pathways (32). Loss of RDE-10 reduces the production of 22G RNAs downstream of exogenous dsRNA and downstream of endogenous small RNAs called 26G RNAs that are 26-nt long and have a 5' G (21, 22). Current models for the production of 26G RNAs (38, 39) propose that the RdRP RRF-3 transcribes long antisense RNA from internal C nucleotides on template mRNA, the phosphatase PIR-1 converts the 5' triphosphate of the RdRP product into 5' mono phosphate, the template is then trimmed by the 3'-5' exonuclease ERI-1 to generate a blunt-ended dsRNA, which is then cleaved by DCR-1 to generate the mature 26G RNAs that are bound by the Argonaute ERGO-1. While a similar preference by RdRPs can explain the 5'G bias of the downstream 22G RNAs, the mechanism(s) for generating RNA that are precisely 22 nucleotides long remain unclear. This precision could be achieved either through the trimming of template mRNAs into 22-nt long pieces or through the trimming of secondary small RNAs made by RdRPs into 22-nt long pieces. The detection of long pUG RNAs with no detectable shorter pUG RNAs upstream of sequences matching the dsRNA (Fig. 4) argues against the 3' trimming of mRNA templates to generate shorter RNAs that then get pUGylated to become stabilized templates for RdRPs and against pUG RNA generation driven by successive rounds of 22G RNA production in somatic cells. Furthermore, potential 5' trimming or endonucleolytic cleavage of long pUG RNA to generate a 22-nt template for RdRPs cannot explain the 5' G bias of 22G RNAs. Since Argonautes bind the 5' end of small RNAs and can associate with RNAs of different lengths (40, 25), we suggest a model whereby RDE-10 and downstream Argonautes together play a role in the maturation of 22-nt siRNAs from longer RdRP products.

RDE-10 has a conserved Maelstrom domain that shares homology with the DnaQ-H 3'–5' exonuclease family (41) and the mutation we identified as disrupting silencing by dsRNA (Fig. S1) alters a residue located near the highly conserved ECHC zinc-binding motif. Intriguingly, the Maelstrom domain of RDE-10 shares high structural homology with the 3'-5' exonuclease domain of ERI-1 (Fig S4C) but not the exonuclease domain of MUT-7 (Fig. S4D). ERI-1 can trim single-stranded RNA overhangs in vitro (26), and is required for the production of 26G RNAs (42) and for the maturation of rRNAs (43). While no 3'–5'

exonuclease activity of RDE-10 or its orthologs has been demonstrated, maelstrom domain-containing proteins in insects exhibit single-stranded RNA endonuclease activity in vitro (44). Furthermore, RDE-10 could interact with other parts of the RNA silencing machinery (e.g., the Argonaute ERGO-1 as seen using immunoprecipitation (21, 22)) to recruit nucleases (e.g., NYN family exonucleases such as ERI-9 (45)) that trim pre-22G RNAs to the 22-nt size preferred by Argonaute proteins. In support of such exonucleolytic trimming in conjunction with Argonaute binding, the 3'-5' exonuclease SND1 has been shown to trim the 3' ends of miRNAs bound to AGO1 in *Arabidopsis* (46). Furthermore, piRNA maturation in *Drosophila* and mice suggests a model where piwi-type Argonautes bind the 5' end of the pre-piRNA followed by endonucleolytic cutting and exonucleolytic trimming to generate consistently sized mature piRNAs (47). Finally, human ERI1 can trim Ago2-bound micro RNAs to 19-nt (48).

Therefore, we propose that the production of 22G RNAs in response to the addition of dsRNA occurs as follows: (1) non-processive RdRPs (e.g., RRF-1 (49)) make a heterogenous mixture of short RNAs, (2) 2º Argonautes bind the 5' end of these pre-secondary siRNA, (3) RDE-10 and/or associated protein(s) remove excess 3' sequence to generate 22-nt siRNAs that are effectively retained by the mature siRNA-Argonaute complex. Similar mechanisms could be used to generate other 22G RNAs that are independent of RDE-10 (21, 22). Future studies are needed to test each aspect of the model.

Trade-offs in RNA interference. RNAi is now a widely applied tool for gene silencing in plants, insects, and humans. Like *C. elegans*, plants (37) and some insects (50) have RdRPs that could be used to make 2º siRNAs, but many other animals, including humans, do not have RdRPs and thus are unlikely to produce 2º siRNAs. However, silencing can fade despite the production of 2º siRNAs (Fig. 4A), highlighting the importance of dosage for all systems. Two parameters of importance for the acute efficacy of any dsRNA-based drug are the time to knockdown (τ_{kd} in Fig. 3B) and duration of knockdown (t_{kd} in Fig. 3B). The various values of t_{kd} that are possible for each τ_{kd} (Fig. 3C) cautions against using a rapid onset of silencing (low τ_{kd}) as the sole indicator of promise during early stages of drug development when long-term effects of a drug are often not evaluated in the interest of expedience. In short, a drug that takes longer to cause an effect could have a more long-lasting effect. Since a dsRNA drug can be synthesized for any target with equal effort, considerations for the choice of target could be worthwhile because differences in RNA

metabolism between two targets of equal importance can influence the efficacy of the dsRNA drug in all systems. If two genes are at steady state, then the gene with higher mRNA turnover will be more difficult to knockdown because of higher rates of mRNA production (Fig. 3F). Similarly, in the absence of a steady state, a gene undergoing upregulation of transcription, splicing, and/or mRNA export during the administration of the drug will be difficult to knockdown (e.g., Fig. 3E). In the longer term, a concern for any drug is the development of resistance. When a gene with a high threshold for silencing is targeted, it could rely on multiple regulators that act in parallel to contribute to silencing (e.g., *bli-1* in this study), making resistance through the mutation of any one regulator more likely. In contrast, genes with a lower threshold may not require all the regulators for silencing (e.g., *unc-22* in this study), making them ideal targets that remain silenced despite single mutations in many regulators of RNAi (e.g., RDE-10, MUT-16, or NRDE-3 in this study). These trade-offs inform the choice of therapeutic targets and dosage to avoid or delay the development of resistance when using dsRNA-based drugs in agriculture and in human health. The ideal drug would require a minimal dose and use multiple paths to silence the target gene.

Methods Summary. All strains (Table S1) were grown at 20ºC on Nematode Growth Medium (NGM) plates seeded with OP50 *E. coli* (51). Strains with mutations were generated through a genetic screen after mutagenesis using N-ethyl-N-nitrosourea (ENU), using standard genetic crosses (51), or using Cas9-mediated genome editing (52-54). Mutations induced upon ENU exposure were identified using whole genome sequencing (Illumina) followed by analyses of the resultant fastq files. Simulations of the RNAi response were used to identify the domain and range of values consistent with experimental data (Fig. 2) and to explore parameters that support silencing (equilibrium model (Fig. S2) and dynamic model (Figs. 3 and S3)). Feeding RNAi experiments were performed by exposing worms to bacteria that express dsRNA (55) either continuously or for a brief period (Fig. 4A). Multiple sequence alignment (Fig. S4) was performed using Clustal Omega (56) and manually annotated using Illustrator (Adobe). Comparisons of protein structures were performed using AlphaFold predictions (57, 58), pair-wise alignment on Protein Data Bank (59), and the PyMOL Molecular Graphics System (v. 2.4.1 Schrödinger, LLC). Levels of *rde-4* mRNA (Fig. 5E) and pUG RNA (Fig. 4B) were measured using reverse-transcription followed by polymerase chain reaction (RT-PCR). Transgenic strains that express *rde-1(+)* and *rde-4(+)* in specific tissues were generated using Mos1-mediated single copy insertion (MosSCI) (60). Oligonucleotides used are in Table S2. Exact p-values and additional details for each experiment are in Table S3. All code used (R, Python, and Shell) is available at https://github.com/AntonyJose-Lab/Knudsen_et_al_2023.

Acknowledgments

We thank Mary Chey and Julianna Gross for some analysis of mutants from the genetic screen; Zhongchi Liu, Leslie Pick, Norma Andrews, and members of the Jose Lab for comments on the manuscript; and the *Caenorhabditis elegans* Genetic Stock Center for some worm strains. This work was supported in part by National Institutes of Health Grants R01GM111457 and R01GM124356, and National Science Foundation Grant 2120895 to A.M.J.

Materials and Methods

Strains and oligonucleotides used. All strains (listed in Table S1) were cultured on Nematode Growth Medium (NGM) plates seeded with 100 µl of OP50 *E. coli* at 20ºC and strains made through mating were generated using standard methods (51). Oligonucleotides used are in Table S2. Strains generated using Mos1-mediated Single Copy Insertion (MosSCI, ref. (60)) of *rde-4* or *rde-1* rescues in the germline (as in ref. (36)) or of *rde-4* rescues in the hypodermis (27) were used in this study.

Genetic screen. This screen was performed by mutagenizing a strain (AMJ174) with the transgene *T* (*oxSi487[mex-5p::mCherry::H2B::tbb-2 3'UTR::gpd-2 operon::GFP::H2B::cye-1 3'UTR + unc-119(+)]*, (29)) silenced for >200 generations after introducing a mutation in *lin-2(jam30)* (sgRNA (P1), primers (P2, P3, P4) using Cas9-mediated genome editing of AMJ844 (*¡T; dpy-2(e8)*, (29)) while correcting the *dpy-2(e8)* mutation to wild type (creating *dpy-2(jam29)*; sgRNA (P5), primers (P6, P7, P8)). The *lin-2* mutation limits brood size (61) and facilitates screening. Near-starved animals (P0) of all life stages were mutagenized using 1mM N-Ethyl-N-Nitrosourea (ENU, Toronto Research Chemicals) for 4-6 hours. Mutagenized animals were washed four times with wash buffer (0.01% Triton X-100 in M9) and 2-3 adult animals were placed on NG plates seeded with OP50. Over the next 3 weeks, F1, F2, and F3 progeny were screened to isolate mutants that show mCherry fluorescence. These animals were singled out (up to 7 animals from each P0 plate) and tested for the persistence of expression in descendants. Of the 15 viable mutants isolated using this primary screen, five with mutations in *mut-16* were analyzed in this study.

Whole genome sequencing. Libraries were prepared using TruSeq DNA Library Prep kits (Illumina) and samples were sequenced at Omega Biosciences. The fastq files obtained after Illumina sequencing (1x PE 150 b, Omega Biosciences) were analyzed to identify candidate mutations responsible for the observed defects in the sequenced strains. For each strain, sequences were trimmed using cutadapt (v. 3.5), mapped to the *C. elegans* genome (WBcel235/ce11) using bowtie2 (v. 2.4.2), sorted using samtools (v. 1.11), and the resulting .bam file was analyzed to call variants using snpEff (v. 5.0e). The variants classified as 'HIGH' or 'MODERATE' in the .ann.vcf file for each strain that were not shared by any two or more strains were culled as new mutations caused by mutagenesis in each strain. These new mutations in each strain were compared with those of all other strains ('in silico complementation') using a custom script to identify sets of strains with different mutations in the same genes. Specific details for each

step are provided within the scripts '1_fastq_to_sorted_bam.sh', '2_sorted_bam_to_mutated_genes.sh', '3_in_silico_complementation.sh' available at GitHub (https://github.com/AntonyJose-Lab/Knudsen_et_al_2023). Raw fastq files for the strains analyzed in this study (AMJ1023, AMJ1025, AMJ1035, AMJ1042, and AMJ1091) have been submitted to SRA (PRJNA928750).

Modeling and simulation. The RNAi response was explored using three models of increasing complexity: (1) a single-network model of protein factors with branching pathways for RNA amplification and subsequent gene silencing (Fig. 2); (2) an equilibrium model for the dependence of mRNA and pre-mRNA on small RNAs and other RNA intermediates (Fig. S2); and (3) a dynamic model using ordinary differential equations for the dependence of mRNA and pre-mRNA on small RNAs and other RNA intermediates (Fig. 3 and S3). Simulations of single network and exploration of equilibrium model were conducted in R (v. 3.6.3). Simulations of the dynamic model were conducted in Python (v. 3.8.5) and in R (v. 4.1.0).

Single network: Random numbers from 0 to 2 were selected for each of the assigned variables ($\mathcal{N}m$, $\mathcal{N}r$, $\mathcal{O}m$, $\mathcal{O}r$) and parameter sets that satisfy experimental constraints were plotted. Specific details are provided within the script '2022_6_13_RNAi_in_Celegans_linear_modified.R' available at GitHub (https://github.com/AntonyJose-Lab/Knudsen_et_al_2023).

Equilibrium model: This model for RNAi interference assumes that all reactions have reached equilibrium. Additional assumptions include (1) 1º siRNAs, then pUG RNAs, then 2º siRNAs are made sequentially, (2) no 3º siRNAs are produced for these somatic targets (supported by ref. (18)), (3) there is no recycling of full-length mRNA or full-length pre-mRNA after small RNA binding, and (4) there are no other mechanisms for the turnover of the RNA species considered in the timescale considered. Specific details are provided within the script '2022_2_9_RNAi_network_thresholds_simpler.R' available at GitHub (https://github.com/AntonyJose-Lab/Knudsen_et_al_2023).

Dynamic model: A series of differential equations were used to describe the rate of change for dsRNA, 1º siRNAs, mRNAs, pre-mRNAs, pUG RNAs, and 2º siRNAs, and numerically simulated using the 4th Order Runge-Kutta method. Specific details are provided within the scripts '2022_6_29_Celegans_RNAi_ODEs_RK4_method_d6.py' and

'2022_7_14_RNAiDynamics_ODEs_Parameter_Analysis.R' available at GitHub (https://github.com/AntonyJose-Lab/Knudsen_et_al_2023).

Genome editing. The gonads of adult *C. elegans* were injected with nuclear-localized Cas9 (PNA Bio) preincubated at 37°C for 10 min with a hybridized crRNA/tracrRNA (Integrated DNA Technologies), as well as an oligonucleotide or PCR-amplified homology repair template. Plates with successfully edited F1 animals were screened for Dpy or Rol animals when using *dpy-10* editing as a co-CRISPR (52, 53) or for Rol animals when using the pRF4 plasmid as a co-injection marker (54).

To introduce a premature stop codon in *mut-16:* Injection of a crRNA with the target sequence (P9) (Integrated DNA Technologies), tracrRNA, Cas9, a *mut-16(-)* homology repair template (P10) mimicking the mutation in *mut-16(jam139),* predicted amino acid change Y294*, and *dpy-10* crRNA (P11) and *dpy-10(-)* homology repair template (P12) into N2 or AMJ1489 and subsequent screening were performed as described above. Genotyping for *mut-16(jam148, jam240, jam265, jam266, jam267, or jam268)* was performed using duplex PCR (P13, P14) followed by restriction digestion with BstBI. The nonsense mutations in different strains was verified by Sanger sequencing.

To make the *mut-16(-) rde-10(-)* double mutant: Injection of a crRNA with the target sequence (P15) (Integrated DNA Technologies), tracrRNA, Cas9, a *rde-10(-)* homology repair template (P16) mimicking the mutation in *rde-10(jam248)*, and *dpy-10* crRNA (P11) and *dpy-10(-)* homology repair template (P12) into AMJ1397 (*mut-16(jam148))* and subsequent screening were performed as described above. Genotyping for *rde-10(-)* was performed using duplex PCR (P17, P18) followed by restriction digestion with EcoRV. A strain with a mutation in *rde-10* that results in a 115-bp frameshift followed by an early stop codon was designated as AMJ1470.

To introduce the mutation in *rde-10* that will encode RDE-10(Ser228Phe): Injection of a crRNA with the target sequence (P15) (Integrated DNA Technologies), tracrRNA, Cas9, a *rde-10(-)* homology repair template (P16) mimicking the mutation in *rde-10(jam248)* (Fig. S1), and pRF4 into N2 and subsequent screening were performed as described above. Genotyping for the mutation was performed using duplex PCR (P17, P18) followed by restriction digestion with EcoRV. A strain with the missense mutation verified by Sanger sequencing was designated as AMJ1489.

To introduce a premature stop codon in *nrde-3*: Injection of a crRNA with the target sequence (P19) (Integrated DNA Technologies), tracrRNA, Cas9, a *nrde-3(-)* homology repair template (P20), mimicking *nrde-3(gg066)* (25), and pRF4 into N2 and subsequent screening were performed as described above. Genotyping for *nrde-3(jam205)* was performed using duplex PCR (P21, P22) followed by restriction digestion with AclI. A strain with the nonsense mutation verified by Sanger sequencing was designated as AMJ1510.

To introduce a premature stop codon in *eri-1:* Injection of a crRNA with the target sequence (P23) (Integrated DNA Technologies), tracrRNA, Cas9, an *eri-1(-)* homology repair template (P24), predicted to encode ERI-1(E225*) after the edit, and pRF4 into AMJ1611 or N2 and subsequent screening were performed as described above. Genotyping for *eri-1(jam260, jam261, jam262, jam263, or jam264)* was performed using duplex PCR (P25, P26) followed by restriction digestion with DpnII. Additionally, when *eri-1(mg366)* was crossed with other mutants, duplex PCR with P27 and P28 was used for genotyping.

Sequence and structure alignments. Sequences of *C. elegans* proteins were obtained from WormBase; sequences of proteins from all other species were obtained from UniProt. Alignments were created using Clustal Omega (EMBL-EBI) with default settings.

PyMOL (v. 2.4.1) was used to modify and annotate PDB files. The RDE-10 (UniProt: Q9N3S2) PDB file is based on predictions from AlphaFold. Protein domains were colored based on homology to domains as found in the EMBL-EBI Pfam database (Maelstrom: PF13017). The protein structure alignment was done using the Pairwise Structure Alignment from Protein Data Bank with rigid parameters (RMSD Cutoff 3; AFP Distance Cutoff: 1600; Fragment length: 8). The exonuclease domain of ERI-1 (UniProt:O444606) and of MUT-7 (UniProt:P34607) were compared with the Maelstrom domain of RDE-10.

Feeding RNAi. Control RNAi by feeding *E. coli* containing the empty dsRNA-expression vector (L4440), which can generate a short dsRNA derived from the multiple cloning site but does not produce dsRNA against any *C. elegans* gene, was done in parallel with all RNAi assays.

P0 and F1 feeding: Bacteria expressing dsRNA was cultured in LB media with 100 µg/µl carbenicillin overnight at 37ºC at 250 rpm. 100 µl of cultured bacteria was then seeded onto RNAi plates. Adult animals were passaged onto seeded RNAi plates and removed after 24hr. Progeny were scored for

silencing by bacteria expressing dsRNA targeting *unc-22* (defect evident as twitching within ~3 min. in 3 mM levamisole) or *bli-1* (defect evident as blisters along the body).

P0 Pulse feeding: L4 and young adult animals were placed on seeded RNAi plates for 1hr after which they were transferred to an OP50 plate for 1hr, and then transferred to a new OP50 plate once again to minimize the residual RNAi food carryover. Animals were left on OP50 plates and scored every 24hr for 8 subsequent days with transfer to new OP50 plates every two days to prevent overcrowding.

F1 only feeding: A single L4 or young adult (1 day older than L4) animal (P0) was placed on an RNAi plate seeded with 5µl of OP50 and allowed to lay eggs. After 1 day, when most of the OP50 was eaten, the P0 animal was removed, leaving the F1 progeny. 100µl of an overnight culture of RNAi food (*E. coli* which express dsRNA against a target gene) was added to the plate. Two or three days later, the F1 animals were scored for gene silencing by measuring gene-specific defects.

RNA extraction and PCR with reverse transcription (RT-PCR). Total RNA was extracted using TRIzol (Fisher Scientific) from pellets of mixed-stage animals collected from non-starved but crowded plates in biological triplicate for each strain after exposure to either *unc-22* RNAi or the L4440 vector. The aqueous phase was then washed with an equal amount of chloroform and precipitated overnight at -20°C with 10 µg glycogen (Invitrogen) and 1 ml of isopropanol. RNA pellets were washed twice with 70% ethanol and resuspended in 25 µl of nuclease free water.

RT-PCRs for pUG RNAs (Fig. 4B) were done as described earlier (16). Briefly, cDNA was created from isolated RNA using Superscript III Reverse Transcriptase (ThermoFisher) and a universal primer (P29) that contains nine AC repeats and two adapter sequences. The cDNA was used as a template for a Phusion (NEB) PCR with the first set of primers (adapter 1 P30; *gsa-1* P31; 0kb P32; 1kb P33), the amplicon was diluted 1:20 and used as template for the nested Phusion PCR with the second set of primers (adapter 2 P34; *gsa-1* P35; 0kb P36; 1kb P37). The final PCR product (20 µl) was loaded on a 1% agarose gel and imaged. An annealing temperature of 60ºC was used for *gsa-1* and 57ºC was used for all other primer sets.

For semi-quantitative RT-PCR (Fig. 5E), RNA from each strain was isolated from 50 L4-staged animals as described earlier (62). Primer P38 was used to reverse transcribe the sense strand of *rde-4* and P39 was used to reverse transcribe the sense strand of *tbb-2*. The resulting cDNA was used as a template for PCR (30 cycles for both *rde-4* and *tbb-2*) using Taq polymerase and gene-specific primers (P40, P41

for *rde-4* and P42, P43 for *tbb-2*). Intensities of the bands were quantified using Image J (NIH). The relative intensity of the *rde-4* band normalized to that of the *tbb-2* band was set as 1.0 in wild type. The relative normalized intensity of the *rde-4* band in WM49 (*rde-4(ne301)*) was subtracted from that in AMJ611 to report the levels of *rde-4(+)* mRNA (0.3 relative to wild type).

Rationale for inferences. Prior knowledge: Gene-specific requirements for RNA silencing could reflect specialization along pathways as is supposed for multiple endogenous small RNA pathways in *C. elegans*. Reasons that impact the efficiency of silencing a gene are obscure because of a lack of a quantitative model for RNAi that incorporates recently discovered RNA intermediates.

Evidence supporting key conclusions: Three different proteins, MUT-16, RDE-10, and NRDE-3 play a role in RNAi such that each is singly required for silencing *bli-1* but any two is sufficient for silencing *unc-22*. Simulations support the parsimonious hypothesis that this complex redundancy can be explained by quantitative contributions of a single regulatory network for silencing both genes. A quantitative model for RNAi of any gene at steady state reveals several ways that differences in genetic requirements could arise for silencing different genes. Experimental tests that confirm predictions of the quantitative models include recovery from silencing after exposure to a pulse of *unc-22* dsRNA, which supports the turnover of all key RNA intermediates (1º siRNAs, 2º siRNAs, and pUG RNAs) through mechanisms that are currently unknown; the dearth of pUG RNA generation by 2º siRNAs, consistent with a lack of 3º siRNAs; and the bypass of the requirement for NRDE-3 for silencing *bli-1* when the processing of dsRNA is enhanced through the loss of ERI-1 or the overexpression of RDE-4.

References

1. Fire, A., Xu, S., Montgomery, M. K., Kostas, S. A., Driver, S. E., & Mello, C. C. Potent and specific genetic interference by double-stranded RNA in Caenorhabditis elegans. *Nature*, **391**(6669), 806–811 (1998).
2. Das, P. R., & Sherif, S. M. Application of Exogenous dsRNAs-induced RNAi in Agriculture: Challenges and Triumphs. *Front. Plant Sci.*, **11**, 946 (2020).
3. Vogel, E., Santos, D., Mingels, L., Verdonckt, T. W., & Broeck, J. V. RNA Interference in Insects: Protecting Beneficials and Controlling Pests. *Front. Physiol.*, **9**, 1912 (2019).
4. Zhu, Y., Zhu, L., Wang, X., & Hongchuan, J. RNA-based therapeutics: an overview and prospectus. *Cell Death Dis.*, **13**, 644 (2022).
5. Seroussi, U., Li, C., Sundby, A. E., Lee, T. L., Claycomb, J. M., & Saltzman, A. L. Mechanisms of epigenetic regulation by C. elegans nuclear RNA interference pathways. *Semin. Cell Dev. Biol.*, **127**, 142–154 (2022).
6. Winston, W. M., Molodowitch, C., & Hunter, C. P. Systemic RNAi in C. elegans requires the putative transmembrane protein SID-1. *Science*, **295**(5564), 2456–2459 (2002).
7. Feinberg, E. H., & Hunter, C. P. Transport of dsRNA into cells by the transmembrane protein SID-1. *Science*, **301**(5639), 1545–1547 (2003).
8. Tabara, H., Yigit, E., Siomi, H., & Mello, C. C. The dsRNA binding protein RDE-4 interacts with RDE-1, DCR-1, and a DExH-box helicase to direct RNAi in C. elegans. *Cell*, **109**(7), 861–871 (2002).
9. Knight, S. W., & Bass, B. L. A role for the RNase III enzyme DCR-1 in RNA interference and germ line development in Caenorhabditis elegans. *Science*, **293**(5538), 2269–2271 (2001).
10. Parker, G. S., Eckert, D. M., & Bass, B. L. RDE-4 preferentially binds long dsRNA and its dimerization is necessary for cleavage of dsRNA to siRNA. *RNA*, **12**(5), 807–818 (2006).
11. Parrish, S., & Fire, A. Distinct roles for RDE-1 and RDE-4 during RNA interference in Caenorhabditis elegans. *RNA*, **7**(10), 1397–1402 (2001).
12. Tabara, H., *et al*. The rde-1 gene, RNA interference, and transposon silencing in C. elegans. *Cell*, **99**(2), 123–132 (1999).

13. Steiner, F. A., Okihara, K. L., Hoogstrate, S. W., Sijen, T., & Ketting, R. F. RDE-1 slicer activity is required only for passenger-strand cleavage during RNAi in Caenorhabditis elegans. *Nat. Struct. Mol. Biol.*, **16**(2), 207–211 (2009).
14. Preston, M. A., *et al*. Unbiased screen of RNA tailing activities reveals a poly(UG) polymerase. *Nat. Methods*, **16**(5), 437–445 (2019).
15. Chen, C. C., *et al*. A member of the polymerase beta nucleotidyltransferase superfamily is required for RNA interference in C. elegans. *Curr. Biol.*, **15**(4), 378–383 (2005).
16. Shukla, A., *et al*. poly(UG)-tailed RNAs in genome protection and epigenetic inheritance. *Nature*, **582**(7811), 283–288 (2020).
17. Pak, J., & Fire, A. Distinct populations of primary and secondary effectors during RNAi in C. elegans. *Science*, **315**(5809), 241–244 (2007).
18. Pak, J., Maniar, J. M., Mello, C. C., & Fire, A. Protection from feed-forward amplification in an amplified RNAi mechanism. *Cell*, **151**(4), 885–899 (2012).
19. Zhang, C., *et al*. mut-16 and other mutator class genes modulate 22G and 26G siRNA pathways in Caenorhabditis elegans. *Proc. Natl. Acad. Sci. USA*, **108**(4), 1201–1208 (2011).
20. Phillips, C. M., Montgomery, T. A., Breen, P. C., & Ruvkun, G. MUT-16 promotes formation of perinuclear mutator foci required for RNA silencing in the C. elegans germline. *Genes Dev.*, **26**(13), 1433–1444 (2012).
21. Yang, H., *et al*. The RDE-10/RDE-11 complex triggers RNAi-induced mRNA degradation by association with target mRNA in C. elegans. *Genes Dev.*, **26**(8), 846–856 (2012).
22. Zhang, C., *et al*. The Caenorhabditis elegans RDE-10/RDE-11 complex regulates RNAi by promoting secondary siRNA amplification. *Curr. Biol.*, **22**(10), 881–890 (2012).
23. Uebel, C. J., *et al*. Distinct regions of the intrinsically disordered protein MUT-16 mediate assembly of a small RNA amplification complex and promote phase separation of Mutator foci. *PLoS Genet.*, **14**(7), e1007542 (2018).
24. Yigit, E., *et al*. Analysis of the C. elegans Argonaute family reveals that distinct Argonautes act sequentially during RNAi. *Cell*, **127**(4), 747–757 (2006).

25. Guang, S., *et al*. An Argonaute transports siRNAs from the cytoplasm to the nucleus. *Science*, **321**(5888), 537–541 (2008).
26. Kennedy, S., Wang, D., & Ruvkun, G. A conserved siRNA-degrading RNase negatively regulates RNA interference in C. elegans. *Nature*, **427**(6975), 645–649 (2004).
27. Raman, P., Zaghab, S. M., Traver, E. C., & Jose, A. M. The double-stranded RNA binding protein RDE-4 can act cell autonomously during feeding RNAi in C. elegans. *Nucleic Acids Res.*, **45**(14), 8463–8473 (2017).
28. Zhuang, J. J., & Hunter, C. P. Tissue specificity of Caenorhabditis elegans enhanced RNA interference mutants. *Genetics*, **188**(1), 235–237 (2011).
29. Devanapally, S., *et al*. Mating can initiate stable RNA silencing that overcomes epigenetic recovery. *Nat. Commun.*, **12**(1), 4239 (2021).
30. Timmons, L., & Fire, A. Specific interference by ingested dsRNA. *Nature*, **395**(6705), 854 (1998).
31. Bergstrom, C. T., McKittrick, E., & Antia, R. Mathematical models of RNA silencing: unidirectional amplification limits accidental self-directed reactions. *Proc. Natl. Acad. Sci. USA*, **100**(20), 11511–11516 (2003).
32. Gu, W., *et al*. Distinct argonaute-mediated 22G-RNA pathways direct genome surveillance in the C. elegans germline. *Mol. Cell*, **36**(2), 231–244 (2009).
33. Sandy, P., Ventura, A., & Jacks, T. Mammalian RNAi: a practical guide. *Biotechniques*, **39**(2), 215–224 (2005).
34. Sapetschnig, A., Sarkies, P., Lehrbach, N. J., & Miska, E. A. Tertiary siRNAs mediate paramutation in C. elegans. *PLoS Genet.*, **11**(3), e1005078 (2015).
35. Lee, R. C., Hammell, C. M., & Ambros, V. Interacting endogenous and exogenous RNAi pathways in Caenorhabditis elegans. *RNA*, **12**(4), 589–597 (2006).
36. Marré, J., Traver, E. C., & Jose, A. M. Extracellular RNA is transported from one generation to the next in Caenorhabditis elegans. *Proc. Natl. Acad. Sci. USA*, **113**(44), 12496–12501 (2016).
37. Sanan-Mishra, N., Abdul Kader Jailani, A., Mandal, B., & Mukherjee, S. K. Secondary siRNAs in Plants: Biosynthesis, Various Functions, and Applications in Virology. *Front. Plant Sci.*, **12**, 610283 (2021).

38. Blumenfeld, A. L., & Jose, A. M. Reproducible features of small RNAs in C. elegans reveal NU RNAs and provide insights into 22G RNAs and 26G RNAs. *RNA*, **22**(2), 184–192 (2016).
39. Chaves, D. A., *et al*. The RNA phosphatase PIR-1 regulates endogenous small RNA pathways in C. elegans. *Mol. Cell*, **81**(3), 546–557.e5 (2021).
40. Ruby, J. G., *et al*. Large-scale sequencing reveals 21U-RNAs and additional microRNAs and endogenous siRNAs in C. elegans. *Cell*, **127**(6), 1193–1207 (2006).
41. Zhang, D., Xiong, H., Shan, J., Xia, X., & Trudeau, V. L. Functional insight into Maelstrom in the germline piRNA pathway: a unique domain homologous to the DnaQ-H 3'-5' exonuclease, its lineage-specific expansion/loss and evolutionarily active site switch. *Biol. Direct*, **3**, 48 (2008).
42. Duchaine, T. F., *et al*. Functional proteomics reveals the biochemical niche of C. elegans DCR-1 in multiple small-RNA-mediated pathways. *Cell*, **124**(2), 343–354 (2006).
43. Gabel, H. W., & Ruvkun, G. The exonuclease ERI-1 has a conserved dual role in 5.8S rRNA processing and RNAi. *Nat. Struct. Mol. Biol.*, **15**(5), 531–533 (2008).
44. Matsumoto, N., *et al*. Crystal Structure and Activity of the Endoribonuclease Domain of the piRNA Pathway Factor Maelstrom. *Cell Rep.*, **11**(3), 366–375 (2015).
45. Tsai, H. Y., *et al*. A ribonuclease coordinates siRNA amplification and mRNA cleavage during RNAi. *Cell*, **160**(3), 407–419 (2015).
46. Chen, J., *et al*. Structural and biochemical insights into small RNA 3' end trimming by Arabidopsis SDN1. *Nat. Commun.*, **9**(1), 3585 (2018).
47. Stoyko, D., Genzor, P., & Haase, A. D. Hierarchical length and sequence preferences establish a single major piRNA 3'-end. *iScience*, **25**(6), 104427 (2022).
48. Sim, G., *et al*. Manganese-dependent microRNA trimming by 3'→5' exonucleases generates 14-nucleotide or shorter tiny RNAs. *Proc. Natl. Acad. Sci., USA*, **119**(51), e2214335119 (2022).
49. Aoki, K., Moriguchi, H., Yoshioka, T., Okawa, K., & Tabara, H. In vitro analyses of the production and activity of secondary small interfering RNAs in C. elegans. *EMBO J.*, **26**(24), 5007–5019 (2007).
50. Pinzón, N., *et al*. Functional lability of RNA-dependent RNA polymerases in animals. *PLoS Genet.*, **15**(2), e1007915 (2019).

51. Brenner S. The genetics of Caenorhabditis elegans. *Genetics*, **77**(1), 71–94 (1974).
52. Arribere, J.A., *et al*. Efficient marker-free recovery of custom genetic modifications with CRISPR/Cas9 in Caenorhabditis elegans. *Genetics,* **198**(3), 837-46 (2014).
53. Paix, A., Folkmann, A., Rasoloson, D., & Seydoux, G. High Efficiency, Homology-Directed Genome Editing in Caenorhabditis elegans Using CRISPR-Cas9 Ribonucleoprotein Complexes. *Genetics*, **201**(1), 47–54 (2015).
54. Dokshin, G.A., Ghanta, K.S., Piscopo, K.M., and Mello, C.C., Robust Genome Editing with Short Single-Stranded and Long, Partially Single-Stranded DNA Donors in *Caenorhabditis elegans. Genetics,* **210**(3), 781-787 (2018).
55. Kamath, R. S., *et al*. Systematic functional analysis of the Caenorhabditis elegans genome using RNAi. *Nature*, **421**(6920), 231–237 (2003).
56. Sievers, F., *et al*. Fast, scalable generation of high-quality protein multiple sequence alignments using Clustal Omega. *Mol. Syst. Biol.*, **7**, 539 (2011).
57. Jumper, J., *et al*. Highly accurate protein structure prediction with AlphaFold. *Nature*, **596**(7873), 583–589 (2021).
58. Varadi, M., *et al*. AlphaFold Protein Structure Database: massively expanding the structural coverage of protein-sequence space with high-accuracy models. *Nucleic Acids Res.*, **50**(D1), D439–D444 (2022).
59. Zhang, Y., & Skolnick, J. TM-align: a protein structure alignment algorithm based on the TM-score. *Nucleic Acids Res.*, **33**(7), 2302–2309 (2005).
60. Frøkjær-Jensen, C., Davis, M. W., Ailion, M. & Jorgensen, E. M. Improved Mos1-mediated transgenesis in *C. elegans*. *Nat. Methods*, **9**, 117–118 (2012).
61. Ferguson, E. L., & Horvitz, H. R. Identification and characterization of 22 genes that affect the vulval cell lineages of the nematode Caenorhabditis elegans. *Genetics*, **110**(1), 17–72 (1985).
62. Jobson, M. A., *et al*. Transgenerational Effects of Early Life Starvation on Growth, Reproduction, and Stress Resistance in Caenorhabditis elegans. *Genetics*, **201**(1), 201–212 (2015).

Figures

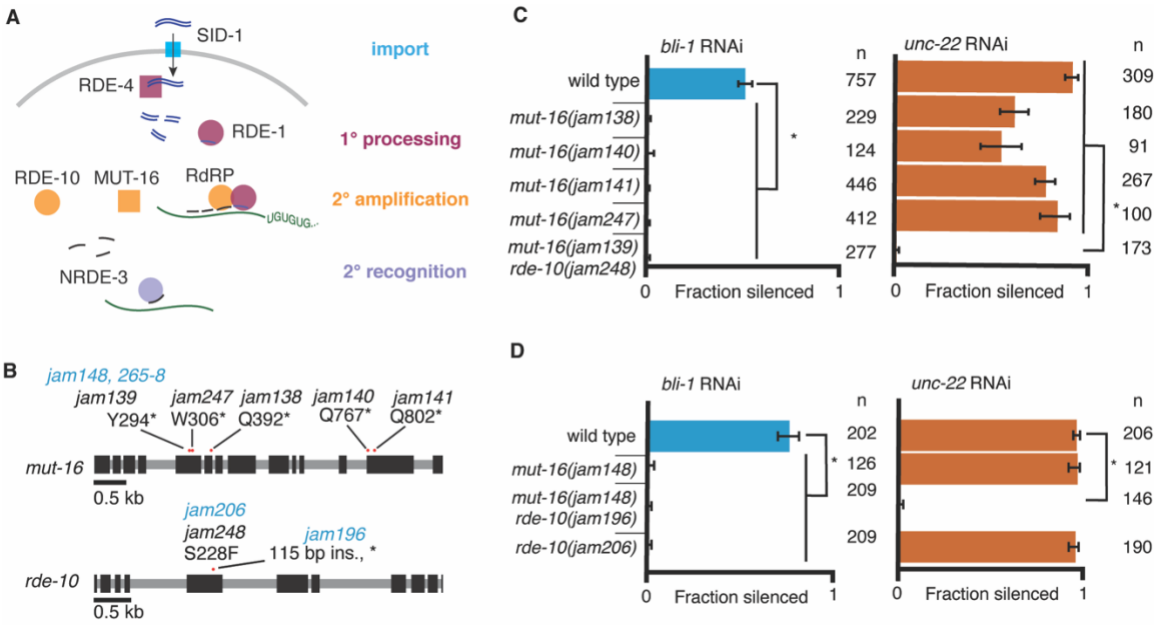

Fig. 1. RNA interference of two somatic targets show stark differences in their requirements for MUT-16 and RDE-10. (A) Overview of RNA interference in somatic cells. Double-stranded RNA (dsRNA, blue) enters the cell through the importer SID-1 (import, teal), after which it is processed by the dsRNA-binding protein RDE-4 and the endonuclease Dicer into 1° short interfering RNAs (siRNAs) that are bound by the primary Argonaute RDE-1 (1º processing, pink). mRNA transcripts (green) recognized by these 1º siRNAs are modified after cleavage by the 3' addition of UG repeats (pUG RNA) and act as templates for the amplification of 2° siRNAs aided by the intrinsically disordered protein MUT-16, the Maelstrom-domain containing protein RDE-10, and RNA-dependent RNA polymerases (2º amplification, orange). These 2° siRNAs can bind secondary Argonaute(s) (e.g., NRDE-3), which can then recognize additional complementary targets (2º recognition) and cause gene silencing. See text for details. (B) Gene schematics depicting the mutant alleles found in a genetic screen (black) and/or created using genome editing (blue). Black boxes indicate exons and red dots indicate locations of mutations. Allele names (e.g., *jam139*) and expected amino acid change in the corresponding proteins (e.g., mutation of a tyrosine codon to a stop codon, Y294*) are indicated. See Fig. S1 for details of genetic screen. (C and D) Response to *bli-1* or *unc-22* RNAi in different mutants. For each mutant, the fraction of animals that showed *bli-1* silencing or *unc-22* silencing (fraction silenced) and the numbers of animals scored (n) are shown. Asterisks indicate p <

0.05 for each comparison (brackets) using Wilson's estimates with continuity correction and error bars represent 95% confidence interval. (C) Of five isolates with a mutation in *mut-16*, four (*jam138*, *jam140*, *jam141*, and *jam247*) failed to silence *bli-1* (blue), but retained *unc-22* silencing (orange). The other mutant failed to silence both genes and additionally had a mutation in *rde-10* (*mut-16(jam139) rde-10(jam248)*). (D) Mutants created using genome editing recapitulated the selective silencing of *unc-22* in *mut-16(-)* single mutants (*mut-16(jam148)*) and the failure to silence both genes in *mut-16(-) rde-10(-)* double mutants (*mut-16(jam148) rde-10(jam206)*). Using genome editing to recreate the *jam248* mutation, which is expected to make a mutant protein (RDE-10(S228F)) that disrupts the Maelstrom domain (see Fig. S1), resulted in animals (*rde-10(jam196)*) that showed *unc-22* silencing but not *bli-1* silencing.

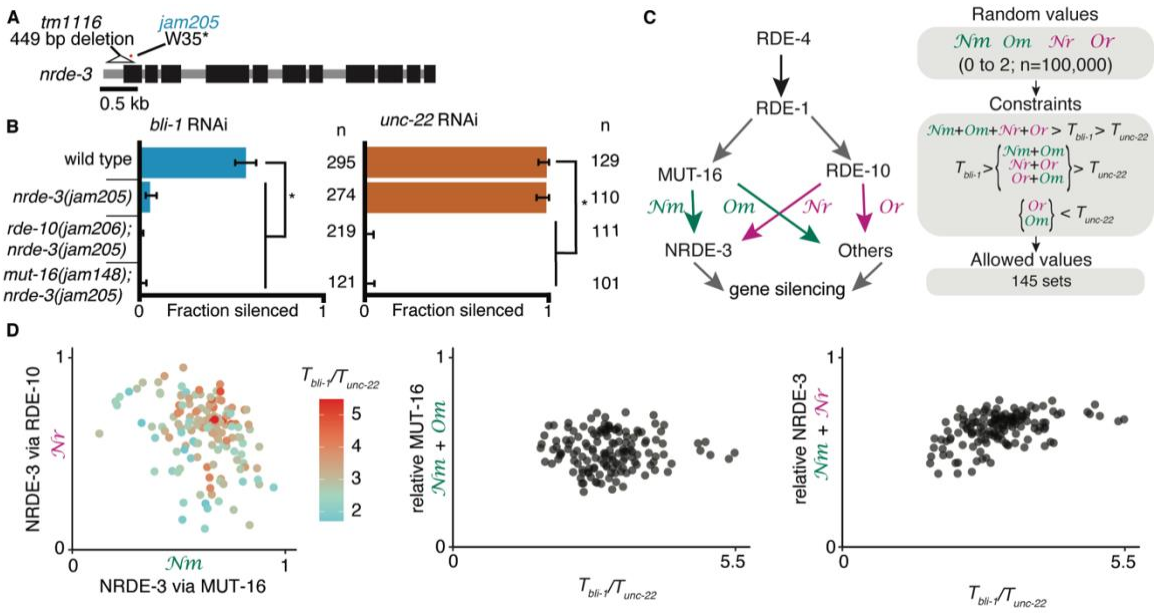

Fig. 2. Gene-specific requirements and complex redundancy can arise from a single RNA regulatory network. (A) Schematic (as in Fig. 1) depicting *nrde-3* alleles. (B) Feeding RNAi of *bli-1* and *unc-22.* Fractions silenced, numbers scored, comparisons, asterisks, and error bars are as in Fig. 1. Single mutants lacking NRDE-3 (*nrde-3(jam205)*) fail to silence *bli-1* but not *unc-22*. Double mutants fail to silence both targets. (C and D) Mutual constraints among parameters required for a single RNA regulatory network to support experimental results. (C, left) Model for a single network of interactors that regulate all RNAi targets. All targets require import (SID-1) and processing (RDE-4 and RDE-1) of dsRNA. Branching after 1° siRNA processing results in four distinct paths ($\mathcal{N}m$, $\mathcal{N}r$, $\mathcal{O}m$, $\mathcal{O}r$) that together contribute to gene silencing. (C, *right*) Representation of simulation workflow. First, random values between 0 and 2 were drawn for each of the four variables ($\mathcal{N}m$, $\mathcal{N}r$, $\mathcal{O}m$, $\mathcal{O}r$). Second, constraints were added based on the experimental results in Fig. 2B and Fig. 1D. Third, allowed values that satisfied all experimental conditions were culled. Of 100,000 sets of random values simulated (0 to 2 for $\mathcal{N}m$, $\mathcal{N}r$, $\mathcal{O}m$, $\mathcal{O}r$ and 0 to 100 for the ratio of thresholds $T_{bli\text{-}1}/T_{unc\text{-}22}$), 145 were consistent with all observed responses to RNAi. These allowed numbers reveal the domain of parameter values that support the observed range of gene silencing outcomes using feeding RNAi. (D, *left*) The contribution of NRDE-3 via MUT-16 ($\mathcal{N}m$) versus that via RDE-10 ($\mathcal{N}r$) for different ratios of thresholds for *bli-1* versus *unc-22* silencing ($T_{bli\text{-}1}/T_{unc\text{-}22}$) are shown. (D, *center* and *right*) The relative contributions to silencing that require MUT-16 ($\mathcal{N}m$ + $\mathcal{O}m$, D, *center*) or NRDE-3 ($\mathcal{N}m$ + $\mathcal{N}r$,

D, *right*) do not frequently take extreme values and both support a low value for the ratio of thresholds ($T_{bli\text{-}1}/T_{unc\text{-}22}$ < ~5.5 despite allowed values of up to 100).

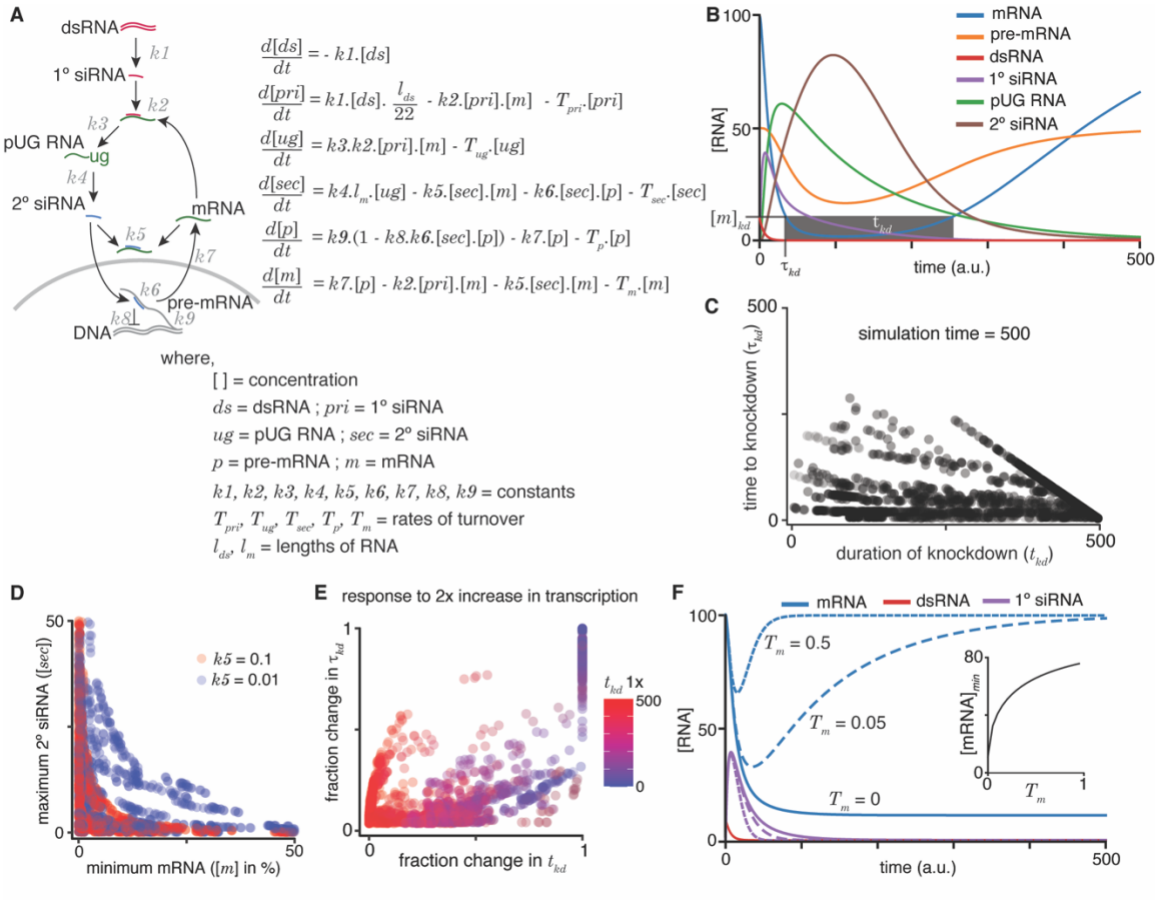

Fig. 3. A quantitative model allows exploration of parameters for RNA interference in *C. elegans*. (A) Schematic (*left*) and ordinary differential equations (*right*) describing the production and turnover of different RNA species. Rate constant for 1º siRNA processing from dsRNA (*k1*), binding constant for 1º siRNA binding target mRNA (*k2*), rate constant for pUG RNA production (*k3*), rate constant for 2º siRNA production (*k4*), binding constant for 2º siRNAs binding mRNA (*k5*) or pre-mRNA (*k6*), rate constant for export and splicing of transcripts from the nucleus (*k7*), rate constant for repression of transcription (*k8*), and rate constant for new transcript production (*k9*). Other terms are described in the figure. (B) Relative changes in the concentrations of each RNA ([RNA] vs. time in a.u.; dsRNA, mRNA, pre-mRNA, pUG RNA, 1º siRNA, and 2º siRNA) for an example set of parameters (all turnover rates = 0.05, *k1* = 1, *k2* = 0.01, *k3* = 1, *k4* = 0.05*l_m = 0.5, *k5* = 0.01, *k6* = 0.01, *k7* = 0.1, *k8* = 0.05, *k9* = 7.5) are illustrated. A reduction to 10% of initial mRNA concentration is designated as the threshold for detecting a defect upon knockdown ($[m]_{kd}$),

the time needed to reach the threshold (τ_{kd}) and the time for which mRNA levels remain below the threshold (t_{kd}) are also indicated. (C) Relationship between the duration of knockdown and the time to knockdown (t_{kd} and τ_{kd} are as in (B)). (D) Relationship between mRNA concentration and 2º siRNA accumulation. The minimum mRNA concentrations and maximum 2º siRNA concentrations reached for different transcripts with two different binding constants of 2º siRNAs binding to mRNA (*k5* = 0.1, red and *k5* = 0.01, blue) are plotted. Also see Fig. S3. (E) Impact of doubling transcription on transcripts with different knockdown parameters. Each transcript is colored based on its initial duration of knockdown (t_{kd}, blue to red gradient) before a 2-fold increase in the rate constant for transcription (*k9*) and the resultant fractional change in the duration of knockdown t_{kd} is plotted against that in the time to knockdown τ_{kd}. (F) Genes with higher turnover are harder to knockdown. Response of mRNAs and their respective 1º siRNA with the same steady-state concentrations but with different rates of mRNA turnover (solid lines: T_m = 0, large dashes: T_m = 0.05, small dashes: T_m = 0.5) upon addition of 10 molecules of dsRNA are shown. (*inset*) Relationship of the minimum concentration of mRNA ([mRNA]$_{min}$) to its T_m in response to a fixed amount of dsRNA.

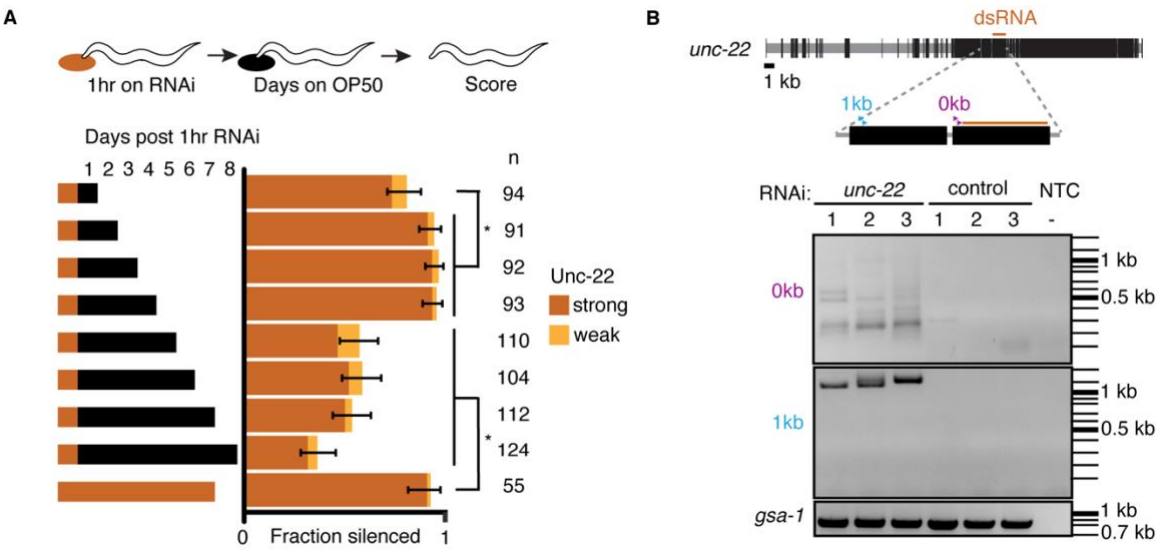

Fig. 4. Animals recover from a pulse of RNAi and production of pUG RNAs is restricted despite continuous exposure to dsRNA. (A) Response to a pulse of feeding RNAi. (*top*) Schematic of assay. Animals were exposed to *unc-22* RNAi for one hour and then returned to OP50 plates. (*bottom*) A separate cohort of animals was scored for silencing after each subsequent 24hr period. Fractions silenced, numbers scored, comparisons, asterisks, and error bars are as in Fig. 1. A weak Unc-22 defect indicates animals that were nearly completely still except for a slight twitch in the head or in the tail. (B) pUG RNA production in response to continuous exposure to *unc-22* dsRNA. (*top*) Schematic depicting the PCR primers used to detect pUG RNAs using RT-PCR. Two sets of primers (0kb, purple; 1kb, blue) positioned 5' of the *unc-22*-dsRNA (orange) were used. (*bottom*) Distribution of DNA amplified from pUG RNAs. Lanes with PCR products amplified from total RNA of animals fed *unc-22* dsRNA (*unc-22*) or L4440 dsRNA (control) isolated from three biological replicates each (1-3), or a no-template control (NTC) with no added RNA (-) are shown. Different bands are detected for each primer set (0kb, top vs. 1kb, bottom). A genomically encoded poly-UG sequence (*gsa-1*) serves as a loading control.

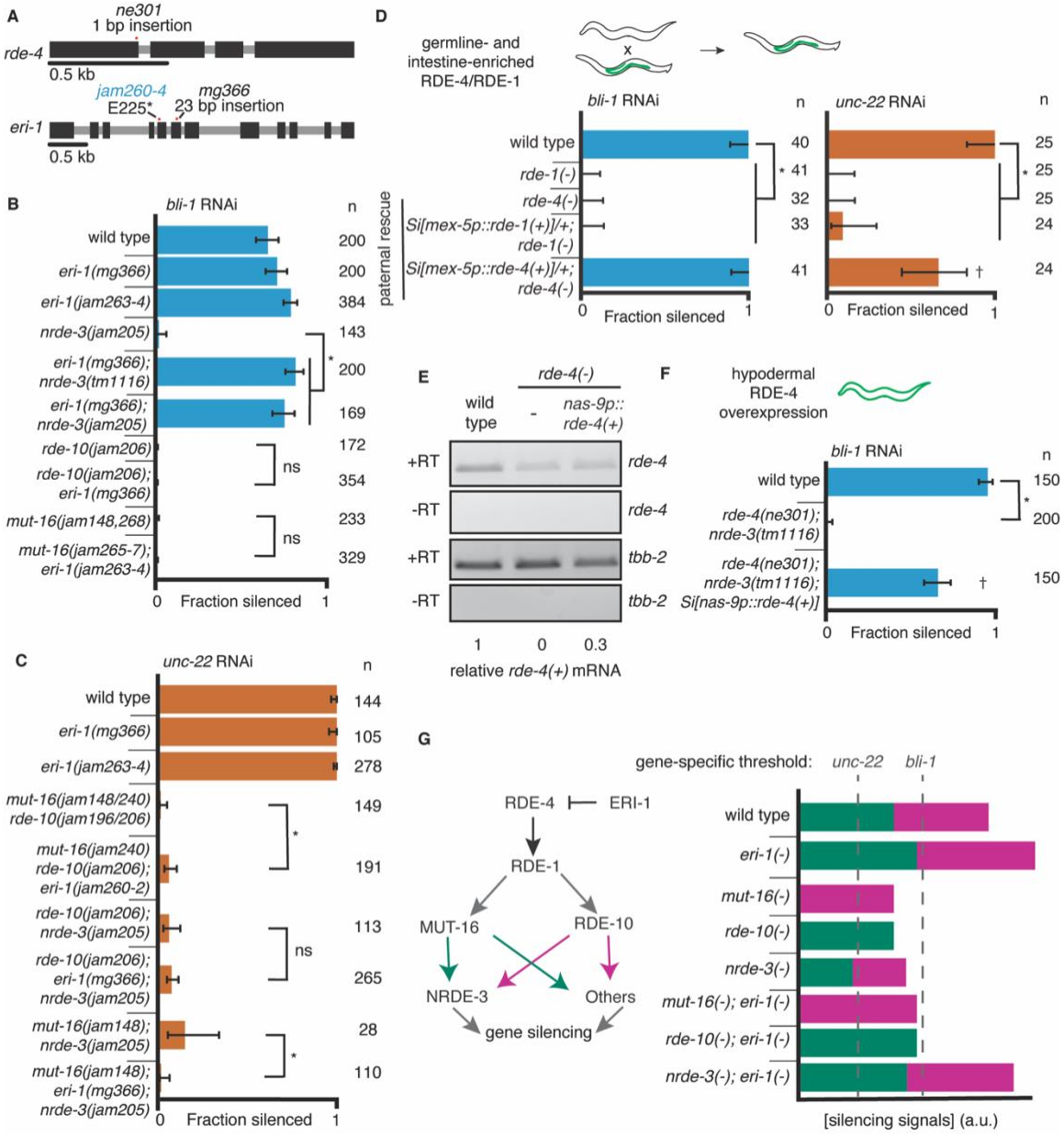

Fig. 5. Gene-specific requirements for regulators of RNA silencing can be bypassed in two ways. (A) Gene schematics (as in Fig. 1) of *rde-4* and *eri-1*. (B and C) Loss of ERI-1 can bypass requirements for silencing *bli-1* but not for silencing *unc-22*. Feeding RNAi targeting *bli-1* (B) or *unc-22* (C) with fractions silenced, numbers scored, comparisons, asterisks, and error bars as in Fig. 1. (B) Loss of ERI-1 (*mg366, jam263,* and *jam264* alleles) can compensate for the role of NRDE-3 (*tm1116* and *jam205* alleles) but not of RDE-10 (*jam206* allele) or MUT-16 (*jam148*, *jam265*, *jam266*, *jam267*, and *jam268* alleles) in *bli-1* silencing. See Table S3 for additional information. (C) Silencing of *unc-22* is not restored by loss of ERI-1

(*mg366*, *jam260*, *jam261*, and *jam262* alleles) in mutants that also lack any two of *mut-16* (*jam148* and *jam240* allele), *rde-10* (*jam196* and *jam206* alleles), or *nrde-3* (*jam205* allele). See Table S3 for additional information. (D to F) Overexpression of RDE-4 in the hypodermis can bypass the requirement for NRDE-3 in *bli-1* silencing. (D) Minimal amounts of RDE-4 are sufficient for somatic silencing. (*top*) Schematic depicting generation of male progeny with paternal inheritance of a single-copy transgene (*Si[…]*) that expresses *rde-4(+)* or *rde-1(+)* under the control of the *mex-5* promoter (*mex-5p*) in the germline (green) of *rde-4(-)* or *rde-1(-)* animals, respectively (germline- and intestine-enriched RDE, based on rescue of RNAi in *rde-1(-)* animals (36)). (*bottom*) Male cross progeny with the transgene were scored after feeding only F1 animals, showing that unlike animals with germline- and intestine- enriched RDE-1, animals with similarly enriched RDE-4 can rescue both *unc-22* and *bli-1* silencing. Thus, small amounts of RDE-4 potentially mis-expressed in the hypodermis or a non-autonomous effect of RDE-4 from the germline or intestine is sufficient for silencing in the muscle and hypodermis. † indicates $p<0.05$ when compared to either wild type or the *rde-4(-)* mutant and other symbols are as in (B). (E) Semiquantitative RT-PCR of *rde-4* mRNA and *tbb-2* mRNA (control) in wild-type animals, *rde-4(-)* animals, or *rde-4(-)* animals expressing *rde-4(+)* in the hypodermis using a single-copy transgene (*Si(nas-9p)*). +RT and -RT indicate whether reverse transcriptase was used. The normalized mRNA abundance in *rde-4(-)* animals was subtracted from all lanes. With the observation in (D) and abundance of *rde-4* transcripts in the germline in wild-type animals (*in situ* data from NEXTDB), expression at ~30% of wild type is expected to be an overexpression in the hypodermis. (F) Silencing of *bli-1* is restored in *nrde-3(tm1116)*; *rde-4(ne301)* double mutants when *rde-4(+)* is overexpressed in the hypodermis (*Si[nas-9p::rde-4(+)]*). (G) Summary depicting selective requirements arising from quantitative differences for RNAi of *bli-1* and *unc-22*. (*left*) Schematic showing contributions of MUT-16-dependent (green) and RDE-10-dependent (magenta) silencing signals. (*right*) Relative contributions of MUT-16-dependent and RDE-10-dependent signals ([silencing signals] in arbitrary units (a.u)) in different experimental conditions.

Supplemental Figures and Tables

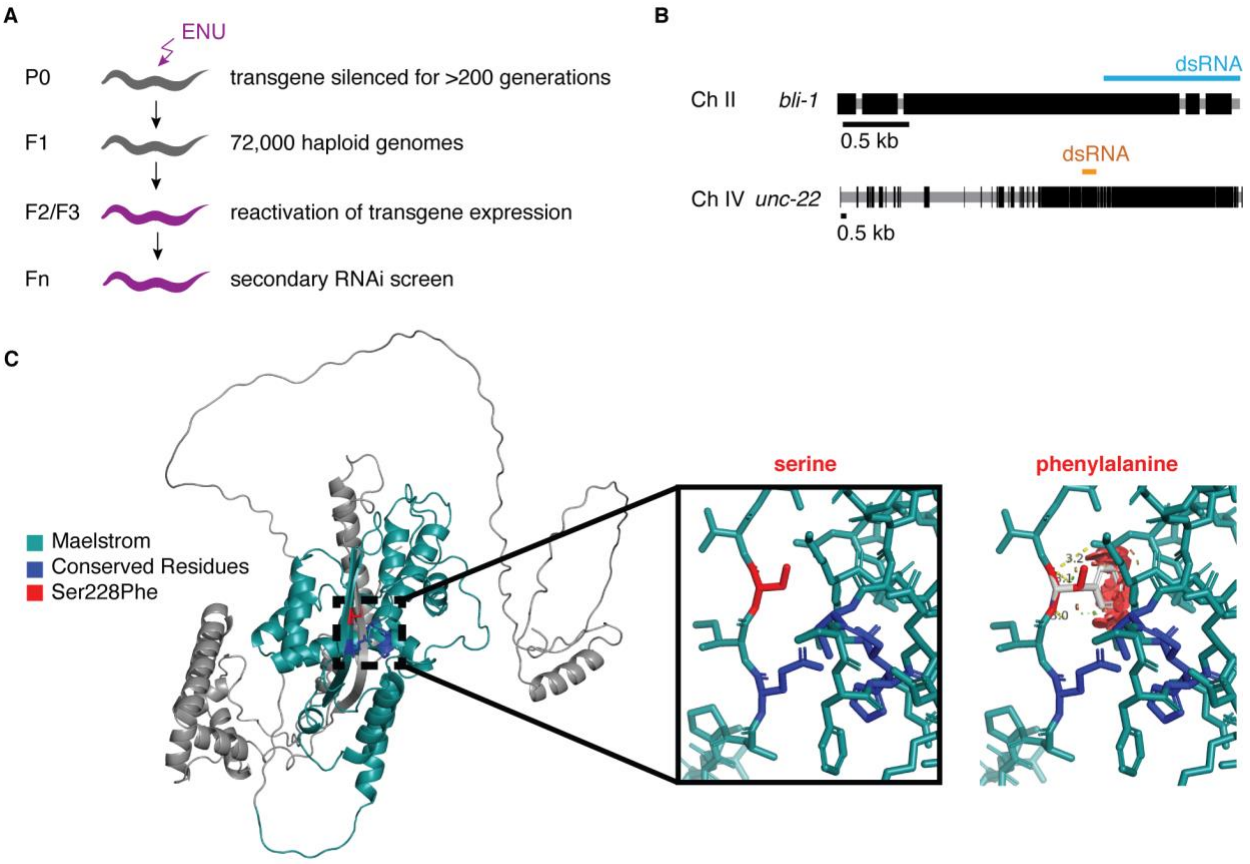

Fig. S1. A forward-genetic screen identifies a mutation that is expected to disrupt the Maelstrom domain of RDE-10. (A) Schematic depicting the screen. Males containing a transgene (*mex-5p::mCherry::h2b::tbb-2 3'utr::gpd-2 operon::gfp::h2b::cye-1 3'utr)* were mated to wild-type hermaphrodites, and progeny that showed silencing of the transgene were isolated. Animals that had been thus silenced for over 200 generations were mutagenized with N-ethyl-N-nitrosourea (ENU). Homozygous mutants that showed a re-activation of the transgene expression were isolated, and then subjected to a secondary feeding RNAi screen where the ability to silence two targets (*bli-1* and *unc-22*) was tested. (B) Schematics depicting the genes that were targeted by feeding RNAi. Black boxes, indicating exons, and regions that share homology with the dsRNA (blue, *bli-1;* orange, *unc-22*) are shown. (C) Predicted structure of RDE-10 showing the expected steric hinderance caused by the Ser228Phe mutation isolated in the screen. (*left*) The structure predicted by AlphaFold (57, 58) contains a Maelstrom domain (teal; Pfam: PF13017). Ser228 (red) and the conserved ECHC motif that can bind zinc (dark blue) are highlighted.

(*middle* and *right*) Closeup of residue 228, showing the wild-type Ser (*middle*) and one orientation of Phe (*right*), which highlights the expected steric hinderance (red).

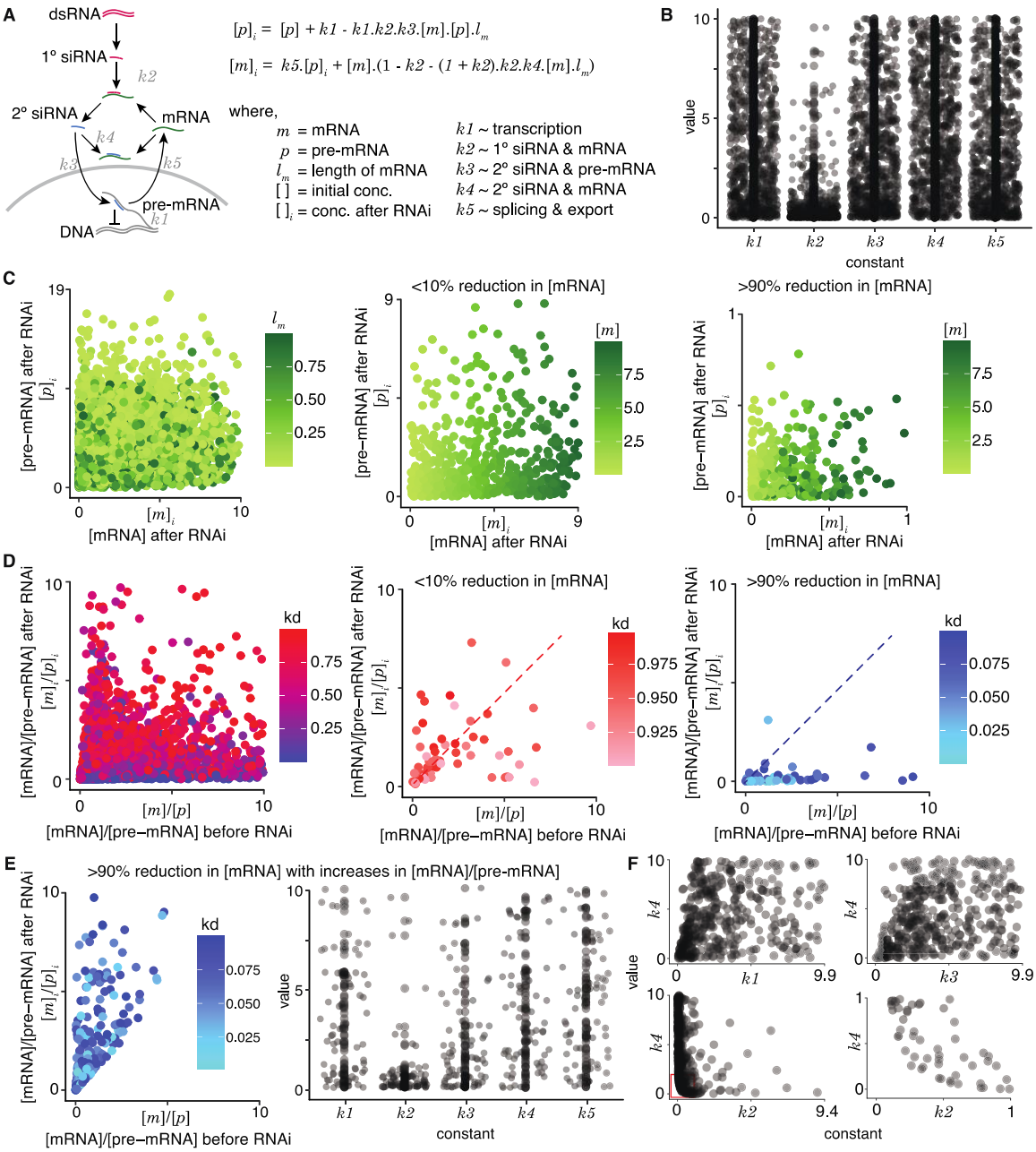

Fig. S2. An equilibrium model for RNAi. (A) Model highlighting different RNA species and their interactions during RNA interference. *Left*, Schematic showing downstream events upon processing of intracellular dsRNA. *Right,* Equations for the pre-mRNA ($[p]_i$) and mRNA ($[m]_i$) concentrations after RNAi in terms of the concentrations before RNAi ($[p]$ and $[m]$) and the length of the transcript (l_m). Rate constants for transcription (*k1*), binding constants for complex formation (1º siRNA-mRNA (*k2*), 2º siRNA-pre-mRNA (*k3*), and 2º siRNA-mRNA (*k4*)), and rate constants for splicing followed by export out of the nucleus (*k5*)

were considered. (B) Distributions of allowed values for all constants that are consistent with knockdown. One million random sets of values from 1 to 10 were assigned for all constants and the 790 sets that supported knockdown ($[m]_i < [m]$) and residual presence of pre-mRNA and mRNA ($[m]_i > 0$ and $[p]_i > 0$) were selected and plotted. Most values of *k2* were small as expected to satisfy the $[m]_i > 0$ constraint because its square is subtracted in the equation for $[m]_i$. (C) RNAi can result in a variety of residual concentrations of pre-mRNA and mRNA. *Left*, Different ratios of residual mRNA and pre-mRNA ($[m]_i/[p]_i$) are possible for a given length of the target mRNA (l_m: 0 to 1). *Middle* and *Right*, Impact of $[m]$ on $[m]_i$ and $[p]_i$. *Middle*, When the knockdown is poor (<10%), the concentrations of mRNA after RNAi ($[m]_i$) remain close to concentrations before RNAi ($[m]$) as expected for all levels of residual pre-mRNA ($[p]_i$) as evidenced by the graded levels of $[m]_i$ that mirror the graded levels of $[m]$. *Right*, When the knockdown is strong (>90%), the low concentrations of mRNA after RNAi ($[m]_i$) can be associated with a range of values for $[p]_i$. (D) RNAi can alter the ratios of pre-mRNA and mRNA. *Left*, Changes in the ratios of mRNA to pre-mRNA upon RNAi ($[m]/[p]$ before to $[m]_i/[p]_i$ after) are possible for a variety of extents of knockdown (kd = $[m]_i/[m]$: 0 to 1). *Middle* and *Right*, Impact of kd on $[m]/[p]$ versus $[m]_i/[p]_i$. Increases and decreases in the ratios of mRNA to pre-mRNA (above versus below the dotted line) can occur in response to both poor (<10% with 0.9 < kd < 1.0, *middle*) and good (>90% with 0.0 < kd < 0.1, *right*) knockdown. While it appears that most cases of efficient knockdown are associated with a decrease in the ratio of mRNA to pre-mRNA (i.e., only one point above dotted line in *right*), increasing the numbers of parameter sets explored could reveal additional examples. (E) (left) Same as in (D, *right*) except only values that were to the left and above the dotted line. Instead of one million simulated values, one hundred million values were simulated to better examine the range of possible values in this group. (*center*) Same as in (B) but for the values culled in (E, *left*). (F) Constants (*k1* to *k5*) do not appear to show strong correlations with one another, except for *k2* and *k4*. The lack of values in the bottom left corner comparing *k2* to *k4* (bottom graphs) reflects the expectation that efficient silencing is not possible when both the primary and secondary binding constants are low.

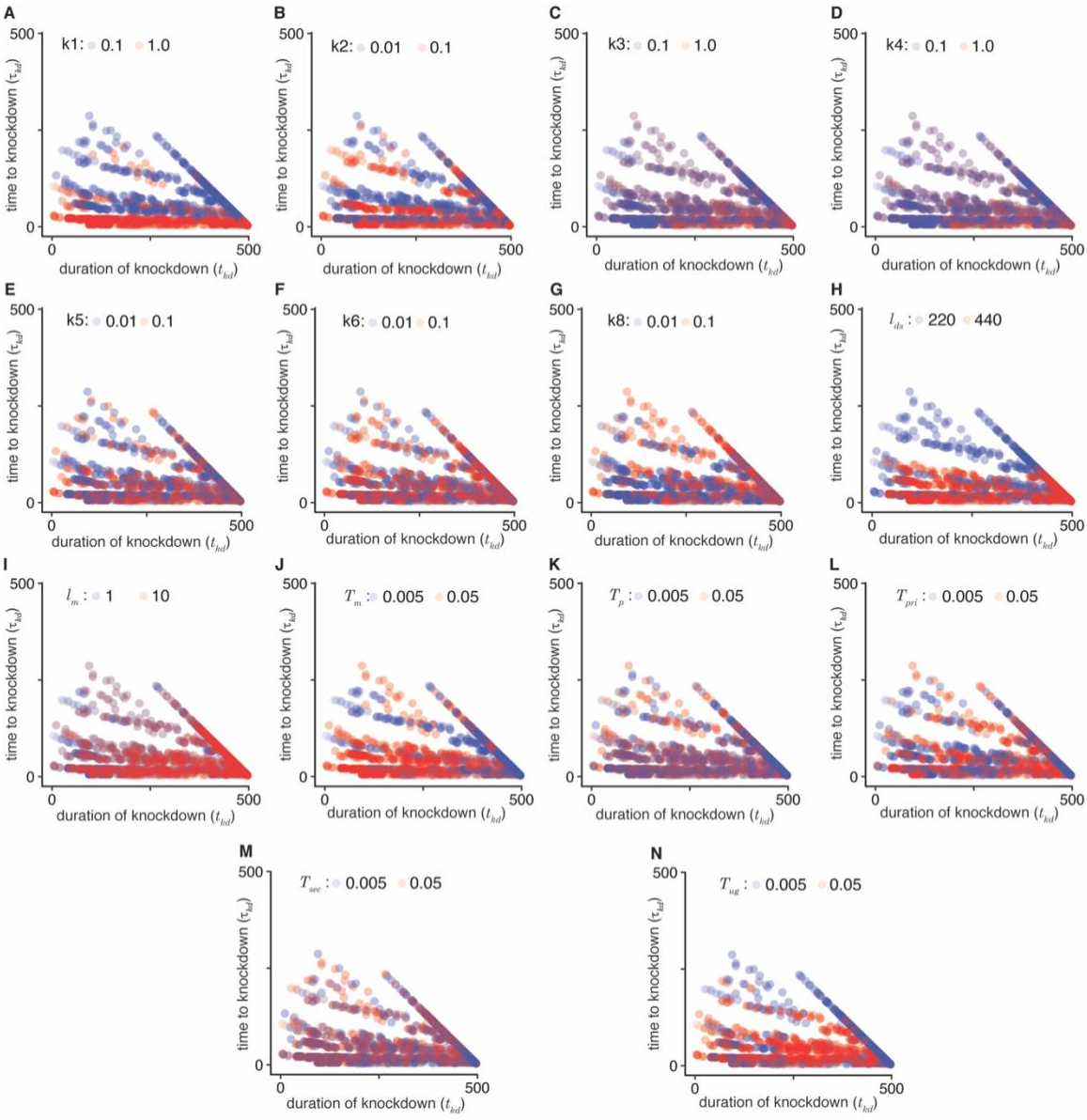

Fig. S3. Impact of model parameters on the time to knockdown (τ_{kd}) and the duration of knockdown (t_{kd}). A low (blue) and high (red) value was selected for each parameter and the τ_{kd} and t_{kd} that result upon similarly varying all other parameters were plotted. Comparisons for 1º siRNA production ((A), *k1* = 0.1 vs. 1.0), recognition of transcripts and1º siRNAs ((B), *k2* = 0.01 vs. 0.1), pUG RNA production ((C), *k3* = 0.1 vs. 1.0), 2º siRNA production ((D), *k4* = 0.1 vs. 1.0), binding of transcripts and 2º siRNAs ((E), *k5* = 0.01 vs. 0.1), transcript maturation, i.e., splicing and export out of the nucleus ((F), *k6* = 0.01 vs. 0.1), downregulation of transcription ((G), *k8* = 0.01 vs. 0.1), length of dsRNA ((H), l_{ds} = 220 vs. 440), length of target mRNA ((I),

l_m = 1 vs. 10), mRNA turnover ((J), T_m = 0.005 vs. 0.05), pre-mRNA turnover ((K), T_p = 0.005 vs. 05), 1º siRNA turnover ((L), T_{pri} = 0.005 vs. 0.05), 2º siRNA turnover ((M), T_{sec} = 0.005 vs. 0.05), and pUG RNA turnover ((N), T_{ug} = 0.005 vs. 0.05) are shown.

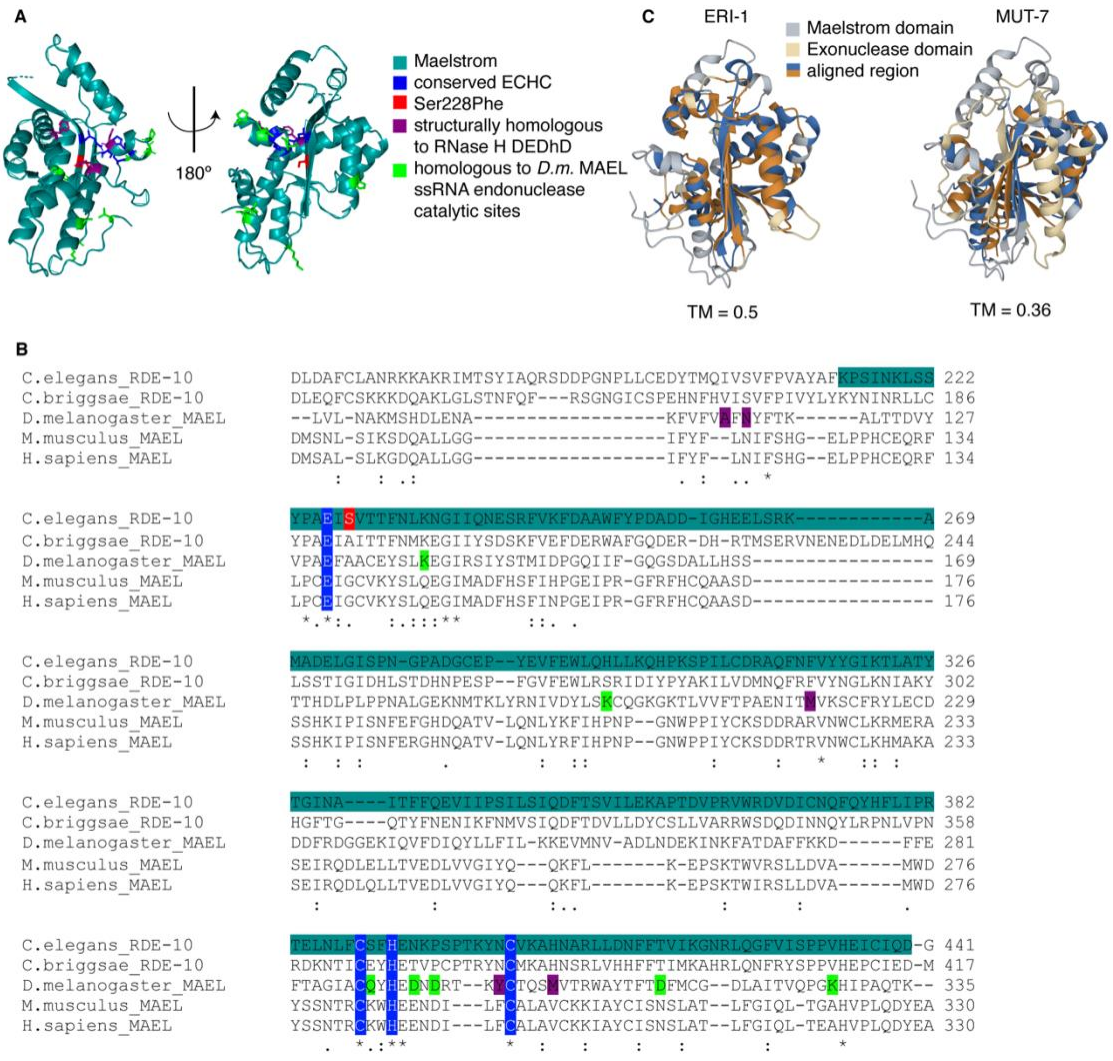

Fig. S4. The predicted structure of the Maelstrom domain of RDE-10 is similar to that of the 3'-5' exonuclease ERI-1. (A) Predicted structure of the Maelstrom domain (teal; Pfam: PF13017) of RDE-10. RDE-10 residues were colored based on studies of the *Drosophila* MAEL protein (44). The zinc-binding ECHC motif (dark blue), the Serine residue mutated in *rde-10(jam248)* (red), residues homologous to the catalytic residues of the Lassa virus exonuclease (purple), and residues homologous to those required for single-stranded RNA endonuclease activity (green) are shown. (B) Alignment of maelstrom domain-containing proteins from multiple species. Asterisks indicate conserved residues, colon indicates residues with strongly similar properties and a period indicates residues with weakly similar properties (56). Residues of interest are shaded as in (A). (C) Structural alignments of the Maelstrom domain of RDE-10 with the 3'-

5’ exonuclease domains of ERI-1 (*left*) and MUT-7 (*right*). The template modeling score (TM = 0.5 for ERI-1 and TM = 0.36 for MUT-7) and regions of high homology (blue and orange) are shown.

Table S1. Strains used in this study.

Strain name	Genotype
N2	wild type
AMJ174	*oxSi487[mex-5p::mCherry::H2B::tbb-2 3'UTR::gpd-2 operon::GFP::H2B::cye-1 3'UTR + unc-119(+)] dpy-2(jam29) II; unc-119(ed3)? III; lin-2(jam30) X*
AMJ183	*rde-4(ne301) III; nrde-3(tm1116) X*
AMJ285	*jamSi1 [mex-5p::rde-4(+)] II; rde-4(ne301) III*
AMJ345	*jamSi2 [mex-5p::rde-1(+)] II; rde-1(ne219) V*
AMJ489	*nrde-3(tm1116) X; eri-1(mg366) IV*
AMJ611	*jamSi6 [nas-9p::rde-4(+)::rde-4 3'UTR] II; rde-4(ne301) III; nrde-3(tm1116) X*
AMJ1023	*mut-16(jam138) I; oxSi487 dpy-2(jam29) II; unc-119(ed3)? III; lin-2(jam30) X*
AMJ1025	*mut-16(jam139) rde-10(jam248) I; oxSi487 dpy-2(jam29) II; unc-119(ed3)? III; lin-2(jam30) X*
AMJ1035	*mut-16(jam140) I; oxSi487 dpy-2(jam29) II; unc-119(ed3)? III; lin-2(jam30) X*
AMJ1042	*mut-16(jam141) I; oxSi487 dpy-2(jam29) II; unc-119(ed3)? III; lin-2(jam30) X*
AMJ1091	*mut-16(jam247) I; oxSi487 dpy-2(jam29) II; unc-119(ed3)? III; lin-2(jam30) X*
AMJ1397	*mut-16(jam148) I*
AMJ1470	*mut-16(jam148) rde-10(jam196) I*
AMJ1489	*rde-10(jam206) I*
AMJ1510	*nrde-3(jam205) X*
AMJ1545	*mut-16(jam148) I; nrde-3(jam205) X*
AMJ1568	*rde-10(jam206) I; nrde-3(jam205) X*
AMJ1611	*mut-16(jam240) rde-10(jam206) I*
AMJ1621	*eri-1(mg366) IV; nrde-3(jam205) X*
AMJ1622	*rde-10(jam206) I; eri-1(mg366) IV*
AMJ1623	*rde-10(jam206) I; eri-1(mg366) IV*
AMJ1624	*rde-10(jam206) I; eri-1(mg366) IV; nrde-3(jam205) X*
AMJ1625	*rde-10(jam206) I; eri-1(mg366) IV; nrde-3(jam205) X*

AMJ1631	*mut-16(jam148) I; eri-1(mg366) IV; nrde-3(jam205) X*
AMJ1632	*mut-16(jam148) I; eri-1(mg366) IV; nrde-3(jam205) X*
AMJ1657	*mut-16(jam240) rde-10(jam206) I; eri-1(jam260) IV*
AMJ1658	*mut-16(jam240) rde-10(jam206) I; eri-1(jam261) IV*
AMJ1659	*mut-16(jam240) rde-10(jam206) I; eri-1(jam262) IV*
AMJ1660	*eri-1(jam263) IV*
AMJ1661	*eri-1(jam264) IV*
AMJ1672	*mut-16(jam265) I; eri-1(jam263) IV*
AMJ1673	*mut-16(jam266) I; eri-1(jam264) IV*
AMJ1674	*mut-16(jam267) I; eri-1(jam264) IV*
AMJ1675	*mut-16(jam268) I*
EG6787	*oxSi487 II; unc-119(ed3) III*
GR1373	*eri-1(mg366) IV*
WM27	*rde-1(ne219) V*
WM49	*rde-4(ne301) III*
WM156	*nrde-3(tm1116) X*

Table S2. Oligonucleotides used in this study.

Primer	**Sequence**
P1	atttaggtgacactatagaaatgctcagagatgctcggttttagagctagaaatagcaag
P2	tcactttcttcgtgcgttcc
P3	ggagaaccactcccagaatg
P4	aatcaatcggctgtccacac
P5	atttaggtgacactatagctggatcacctgggaatccgttttagagctagaaatagcaag
P6	aatcgcaaacgagtgggtac
P7	cgggctagatcataatgagg
P8	ggaccacgtggagttccaggacatccaggttttccaggtgacccaggagagtatggaatt
P9	gaatatttttcgaaaatata

P10 cggcacatgcgaatattttccgaaaatagaaggatattcttcaactcgatccagaaaaac

P11 gctaccataggcaccgcatg

P12 cacttgaacttcaatacggcaagatgagaatgactggaaaccgtaccgcatgcggtgcctatggtagcggagcttca catggcttcagaccaacagccta

P13 cacaaacgccaggaaaggaag

P14 catttctgcgttgttgtggacc

P15 gttgtaacggatatctctgc

P16 aagattgaatgttgtaacgaatatttcagcaggatacgatgaaagcttattgattgatgg

P17 ccgaaatccagatgagttcc

P18 gcatctggataaaaccaagc

P19 acaccacgtacaaatgtttg

P20 tgcgtcatccacaccacgtacaaacgtttagggcactgcaaaaaagccatccagccaaca

P21 gactgtgctgacgctgtttt

P22 ctcccagtggctttcgtttt

P23 tgtggacacggaatcagatc

P24 gaaacagtcgatgctgctccatatttccgataggatcttcaacggctgtacacatggatg

P25 cctatgtccgacctgtcaga

P26 caattccggatttctgaagag

P27 cagacctcacgatatgtggaaa

P28 ggaacatatggggcattcg

P29 gctatggctgttctcatggcggcgtcgccatattctacttcacacacacacacacaca

P30 gctatggctgttctcatggc

P31 gagttctacgatcacattct

P32 tgctccgtggagcaactcgc

P33 gagcacactattctgtgcat

P34 ggcgtcgccatattctactt

P35 cacttgctggaaagacaagg

P36 cgcaagcatgctggtttgta

P37	gcattccatctgcaatgcga
P38	cagtgtgcttgtaaatcggc
P39	tgctcttcggcagttgcttc
P40	gcaaagaatcttgcagcatgg
P41	gaacacacccagactgaaga
P42	gacgagcaaatgctcaacg
P43	tcgtcttcggcagttgcttc

Table S3. Summary of statistics.

Figure	Comparison	Total n	Silenced n	p value	Strains	notes
1B *bli-1*	wild type vs *mut-16(jam138)*	757, 229	391, 0	<0.00001, *	EG6787, AMJ1023	pooled EG6787 from separate experiments
1B *bli-1*	wild type vs *mut-16(jam140)*	757, 277	391, 0	<0.00001, *	EG6787, AMJ1035	pooled EG6787 from separate experiments
1B *bli-1*	wild type vs mut-16(jam141)	757, 124	391, 0	<0.00001, *	EG6787, AMJ1042	pooled EG6787 from separate experiments
1B *bli-1*	wild type vs mut-16(jam247)	757, 446	391, 1	<0.00001, *	EG6787, AMJ1091	pooled EG6787 from separate experiments
1B *bli-1*	wild type vs mut-16(jam139) rde-10(jam248)	757, 412	391, 1	<0.00001, *	EG6787, AMJ1025	pooled EG6787 from separate experiments
1B *unc-22*	wild type vs mut-16(jam139) rde-10(jam248)	309, 173	282, 0	<0.00001, *	EG6787, AMJ1025	pooled EG6787 from separate experiments
1B *unc-22*	mut-16(jam138) vs mut-16(jam139) rde-10(jam248)	180, 173	111, 0	<0.00001, *	AMJ1023, AMJ1025	pooled EG6787 from separate experiments
1B *unc-22*	mut-16(jam140) vs mut-16(jam139) rde-10(jam248)	91, 173	50, 0	<0.00001, *	AMJ1035, AMJ1025	pooled EG6787 from separate experiments
1B *unc-22*	mut-16(jam141) vs mut-16(jam139) rde-10(jam248)	267, 173	208, 0	<0.00001, *	AMJ1042, AMJ1025	pooled EG6787 from separate experiments
1B *unc-22*	mut-16(jam247) vs mut-16(jam139) rde-10(jam248)	100, 173	84, 0	<0.00001, *	AMJ1091, AMJ1025	pooled EG6787 from separate experiments
1D *bli-1*	wild type vs mut-16(jam148)	202, 126	159, 0	<0.00001, *	N2, AMJ1397	
1D *bli-1*	wild type vs mut-16(jam148) rde-10(jam196)	202, 209	159, 0	<0.00001, *	N2, AMJ1470	

1D *bli-1*	wild type vs rde-10(jam206)	202, 209	159, 0	<0.00001, *	N2, AMJ1489	
1D *unc-22*	wild type vs mut-16(jam148)	206, 121	204, 119	0.58802, ns	N2, AMJ1397	
1D *unc-22*	wild type vs mut-16(jam148) rde-10(jam196)	206, 146	204, 0	<0.00001, *	N2, AMJ1470	
1D *unc-22*	wild type vs rde-10(jam206)	206, 190	204, 185	0.21023, ns	N2, AMJ1489	
2B *bli-1*	wild type vs nrde-3(jam205)	295, 274	172, 16	<0.00001, *	N2, AMJ1510	
2B *bli-1*	wild type vs rde-10(jam206); nrde-3(jam205)	295, 219	172, 0	<0.00001, *	N2, AMJ1568	
2B *bli-1*	wild type vs mut-16(jam148); nrde-3(jam205)	295, 121	172, 0	<0.00001, *	N2, AMJ1545	
2B *unc-22*	wild type vs nrde-3(jam205)	129, 110	127, 108	0.87221, ns	N2, AMJ1510	
2B *unc-22*	wild type vs rde-10(jam206); nrde-3(jam205)	129, 111	127, 0	<0.00001, *	N2, AMJ1568	
2B *unc-22*	wild type vs mut-16(jam148); nrde-3(jam205)	129, 101	127, 0	<0.00001, *	N2, AMJ1545	
4A	1 vs 2 days post RNAi	94, 91	76, 86	0.00489, *	N2	
4A	1 vs 3 days post RNAi	94, 92	76, 89	0.00062, *	N2	
4A	1 vs 4 days post RNAi	94, 93	76, 89	0.001627, *	N2	
4A	5 days post RNAi versus 7 days on RNAi	110, 55	63, 51	<0.00001, *	N2	
4A	6 days post RNAi versus 7 days on RNAi	104, 55	61, 51	<0.00001, *	N2	
4A	7 days post RNAi versus 7 days on RNAi	112, 55	60, 51	<0.00001, *	N2	
4A	8 days post RNAi versus 7 days on RNAi	124, 55	45, 51	<0.00001, *	N2	
5B	wild type vs eri-1(mg366)	200, 200	134, 145	0.231163, ns	N2, GR1373	N2 from a second experiment showed comparable values (219/304), GR1373 from a second experiment showed comparable values (169/213)
5B	nrde-3(jam205) vs eri-1(mg366); nrde-3(tm1116)	143, 200	3, 167	0.000132, *	N2, AMJ489	

5B	mut-16(148/268) vs mut-16(jam265-7); eri-1(jam263)	172, 354	0, 0	>0.5, ns	AMJ1397, AMJ1675, AMJ1672-4	AMJ1397 (0/110) and AMJ1675 (0/123) were pooled; AMJ1672 (0/130), AMJ1673 (0/88), and AMJ1674 (0/111) were pooled
5B	rde-10(jam206) vs rde-10(jam206); eri-1(mg366)	233, 329	0, 0	>0.5, ns	AMJ1489, AMJ1622, AMJ1623	AMJ1622 (0/171) and AMJ1623 (0/183) were pooled
5B	nrde-3(jam205) vs eri-1(mg366); nrde-3(jam205)	143, 169	3, 130	<0.00001, *	AMJ1510, AMJ1621	
5C	mut-16(jam148/240) rde-10(jam196/206) vs. mut-16(jam240) rde-10(jam 206); eri-1(jam260-2)	149, 191	1, 10	0.01826, *	AMJ1470, AMJ1611, AMJ1657-9	AMJ1470 (0/32) and AMJ1661 (1/116) were pooled; AMJ1657 (9/75), AMJ1658 (0/56), and AMJ1659 (1/50) were pooled
5C	rde-10(jam206); nrde-3(jam205) vs rde-10(jam206); eri-1(mg366); nrde-3(jam205)	113, 265	6, 18	0.58837, ns	AMJ1568, AMJ1624, AMJ1625	AMJ1624 (4/135) and AMJ1625 (14/112) were pooled
5C	mut-16(jam148); nrde-3(jam205) vs mut-16(jam148); eri-1(mg366); nrde-3(jam205)	28, 110	4, 1	0.00072, *	AMJ1545, AMJ1631, AMJ1632	AMJ1631 (1/52) and AMJ1632 (0/57) were pooled
5D *bli-1*	wild type vs rde-1(ne219)	50, 37	41, 0	<0.00001, *	N2, WM27	N2 data from *rde-4(-)* experiment; N2 data from *rde-1(-)* experiment (not shown) is comparable with 41/50 silenced
5D *bli-1*	wild type vs rde-4(ne301)	40, 50	40, 0	<0.00001, *	N2, WM49	N2 data from *rde-4(-)* experiment; N2 data from *rde-1(-)* experiment (not shown) is comparable with 41/50 silenced
5D *bli-1*	wild type vs Si[mex-5p::rde-1(+)]/+; rde-1(ne219)	50, 33	41, 0	<0.00001, *	N2, AMJ345	N2 data from *rde-4(-)* experiment; N2 data from *rde-1(-)* experiment (not shown) is comparable with 41/50 silenced
5D *bli-1*	wild type vs Si[mex-5p::rde-4(+)]/+; rde-4(ne301)	40, 41	40, 41	>0.5, ns	N2, AMJ285	N2 data from *rde-4(-)* experiment; N2 data from *rde-1(-)* experiment (not shown)

						is comparable with 41/50 silenced
5D *unc-22*	wild type vs rde-1(ne219)	25, 25	25, 0	<0.00001, *	N2, WM27	
5D *unc-22*	wild type vs rde-4(ne301)	25, 25	25, 0	<0.00001, *	N2, WM49	
5D *unc-22*	wild type vs Si[mex-5p::rde-1(+)]/+; rde-1(ne219)	25, 24	25, 2	<0.00001, *	N2, AMJ345	
5D *unc-22*	wild type vs Si[mex-5p::rde-4(+)]/+; rde-4(ne301)	25, 24	25, 16	0.001600, †	N2, AMJ285	† indicates statistical significance vs. wild type and vs. *rde-4(ne301)* mutant
5D *unc-22*	rde-4(ne301) vs *Si[mex-5p::rde-4(+)]/+; rde-4(ne301)*	25, 24	0, 16	<0.00001, †	WM49, AMJ285	† indicates statistical significance vs. wild type and vs. *rde-4(ne301)* mutant
5F	wild type vs rde-4(ne301); nrde-3(tm1116)	150, 200	142, 0	<0.00001, *	N2, AMJ183	
5F	wild type vs rde-4(ne301); nrde-3(tm1116); Si[nas-9p::rde-4(+)]	150, 150	142, 98	<0.00001, †	N2, AMJ611	† indicates statistical significance vs. wild type and vs. *rde-4(ne301); nrde-3(tm1116)* mutant
5F	rde-4(ne301); nrde-3(tm1116); vs rde-4(ne301); nrde-3(tm1116); Si[nas-9p::rde-4(+)]	200, 150	0, 98	<0.00001, †	AMJ183, AMJ611	† indicates statistical significance vs. wild type and vs. *rde-4(ne301); nrde-3(tm1116)* mutant